

This discussion paper is/has been under review for the journal Atmospheric Chemistry and Physics (ACP). Please refer to the corresponding final paper in ACP if available.

## Lightning NO<sub>x</sub> production estimation

K. Miyazaki et al.

# Global lightning NO<sub>x</sub> production estimated by an assimilation of multiple satellite datasets

K. Miyazaki<sup>1</sup>, H. J. Eskes<sup>2</sup>, K. Sudo<sup>3</sup>, and C. Zhang<sup>4</sup>

<sup>1</sup>Japan Agency for Marine–Earth Science and Technology, Yokohama 236-0001, Japan

<sup>2</sup>Royal Netherlands Meteorological Institute (KNMI), Wilhelminalaan 10, 3732 GK, De Bilt, the Netherlands

<sup>3</sup>Graduate School of Environmental Studies, Nagoya University, Nagoya, Japan

<sup>4</sup>International Pacific Research Center, University of Hawaii at Manoa, Honolulu, Hawaii, USA

Received: 28 October 2013 – Accepted: 29 October 2013 – Published: 7 November 2013

Correspondence to: K. Miyazaki (kmiyazaki@jamstec.go.jp)

Published by Copernicus Publications on behalf of the European Geosciences Union.

Title Page

Abstract

Introduction

Conclusions

References

Tables

Figures

◀

▶

◀

▶

Back

Close

Full Screen / Esc

Printer-friendly Version

Interactive Discussion



## Abstract

The global source of lightning-produced  $\text{NO}_x$  ( $\text{LNO}_x$ ) is estimated by assimilating observations of  $\text{NO}_2$ ,  $\text{O}_3$ ,  $\text{HNO}_3$ , and  $\text{CO}$  measured by multiple satellite measurements. Included are observations from the Ozone Monitoring Instrument (OMI), Microwave Limb Sounder (MLS), Tropospheric Emission Spectrometer (TES), and Measurements of Pollution in the Troposphere (MOPITT) instruments. The assimilation of multiple chemical datasets with different vertical sensitivity profiles provides comprehensive constraints on the global  $\text{LNO}_x$  source while improving the representations of the entire chemical system affecting atmospheric  $\text{NO}_x$ , including surface emissions and inflows from the stratosphere. The annual global  $\text{LNO}_x$  source amount and  $\text{NO}$  production efficiency are estimated at  $6.3 \text{ Tg N yr}^{-1}$  and  $350 \text{ mol NO flash}^{-1}$ , respectively. Sensitivity studies with perturbed satellite datasets, model and data assimilation settings leads to an error estimate of about  $1.4 \text{ Tg N yr}^{-1}$  on this global  $\text{LNO}_x$  source. These estimates are significantly different from those derived from  $\text{NO}_2$  observations alone, which may lead to an overestimate of the source adjustment. The total  $\text{LNO}_x$  source is predominantly corrected by the assimilation of OMI  $\text{NO}_2$  observations, while TES and MLS observations add important constraints on the vertical source profile. The results indicate that the widely used lightning parameterization based on the C-shape assumption underestimates the source in the upper troposphere and overestimates the peak source height by up to about 1 km over land and the tropical western Pacific. Adjustments are larger over ocean than over land, suggesting that the cloud height dependence is too weak over the ocean in the Price and Rind (1992) approach. The significantly improved agreement between the analysed ozone fields and independent observations gives confidence in the performance of the  $\text{LNO}_x$  source estimation.

## Lightning $\text{NO}_x$ production estimation

K. Miyazaki et al.

Title Page

Abstract

Introduction

Conclusions

References

Tables

Figures



Back

Close

Full Screen / Esc

Printer-friendly Version

Interactive Discussion



## 1 Introduction

Lightning-produced  $\text{NO}_x$  ( $\text{LNO}_x$ ) plays an important role in tropospheric chemistry through influences on ozone formation and oxidation capacity (e.g. Schumann and Huntrieser, 2007, and references therein).  $\text{LNO}_x$  accounts for only about 10–20 % of the global  $\text{NO}_x$  sources, but is the most dominant source in the upper troposphere. A small fraction of  $\text{LNO}_x$  can lead to significant ozone production in the upper troposphere (Thompson et al., 1994), because the  $\text{O}_3$  production efficiency per  $\text{NO}_x$  molecule typically increases with height owing to the longer lifetime of  $\text{NO}_x$  and the highly non-linear dependence of ozone production on  $\text{NO}_x$  (Pickering et al., 1998; Martin et al., 2000; Jenkins and Ryu, 2004). Therefore, accurate estimates of  $\text{LNO}_x$  source strength and its global distribution are important for understanding tropospheric chemical systems and for improving chemical transport models (CTMs).

The lightning and subsequent  $\text{NO}_x$  formation are estimated with the aid of parameterizations in CTMs. Various schemes have been developed for determining the global distribution of flashes and  $\text{LNO}_x$  sources on the basis of assumptions regarding the  $\text{NO}_x$  production efficiency per flash, energy ratio of cloud-to-ground (CG) flashes to intra-cloud (IC) flashes, and vertical source profiles (Schumann and Huntrieser, 2007). The parameterizations are generally too simplified and have large uncertainties. First, the lightning parameterization cannot fully represent the regional variability of lightning activity (e.g. Boccippio, 2002; Jourdain et al., 2010). Second, most studies have assumed that the energy ratio of CG flashes and IC flashes equals 10, but this ratio is likely to have a much smaller value (e.g. DeCaria et al., 2000; Fehr et al., 2004). Third, assumption of a C-shaped vertical  $\text{LNO}_x$  profile, with a first maximum in the upper troposphere and a second maximum in the boundary layer as proposed by Pickering et al. (1998), may place too much  $\text{NO}_x$  near the surface and too little in the middle and upper troposphere (e.g. Ott et al., 2010).

The  $\text{LNO}_x$  sources can be optimized through a top-down approach, in which estimates of the  $\text{LNO}_x$  sources are obtained by finding the best match between model and

ACPD

13, 29203–29261, 2013

### Lightning $\text{NO}_x$ production estimation

K. Miyazaki et al.

Title Page

Abstract

Introduction

Conclusions

References

Tables

Figures

◀

▶

◀

▶

Back

Close

Full Screen / Esc

Printer-friendly Version

Interactive Discussion



**Lightning NO<sub>x</sub>  
production  
estimation**

K. Miyazaki et al.

Title Page

Abstract

Introduction

Conclusions

References

Tables

Figures

◀

▶

◀

▶

Back

Close

Full Screen / Esc

Printer-friendly Version

Interactive Discussion

observations. Tropospheric NO<sub>2</sub> column observations from satellite instruments have been used to constrain the global LNO<sub>x</sub> source (e.g. Boersma et al., 2005; Beirle et al., 2006; Martin et al., 2007; Lin, 2012). In these estimates, however, the mismatches between observed and simulated NO<sub>2</sub> concentrations are influenced by not only the LNO<sub>x</sub> sources but also by other processes such as surface emissions, stratospheric inflows, and chemical production and loss processes. Errors in these processes cause large uncertainties in the LNO<sub>x</sub> source estimates when observations are used to constrain only the LNO<sub>x</sub> sources.

Satellite measurements of chemical species other than NO<sub>2</sub> provide important constraints on the LNO<sub>x</sub> source by constraining the chemical interactions with NO<sub>x</sub> etc and by reducing errors in other chemical species that influence the NO<sub>x</sub> chemistry. Advanced data assimilation techniques, such as four-dimensional variation (4-D-Var) and ensemble Kalman filtering (EnKF), are powerful tools to combine multiple observations with models to obtain comprehensive constraints on LNO<sub>x</sub> sources. The EnKF differs from 4-D-Var by allowing us to take advantage of the detailed chemical processes in a CTM without developing an adjoint code.

Based on the EnKF approach, Miyazaki et al. (2012a) developed a data assimilation system (CHASER-DAS) using a global CTM CHASER (chemical atmospheric general circulation model for study of the atmospheric environment and radiative forcing). CHASER-DAS simultaneously optimizes the LNO<sub>x</sub> sources and the surface emissions of NO<sub>x</sub> and CO as well as the concentrations of 35 chemical species, while taking into account the chemical interactions through error covariance. The simultaneous optimization of several chemical fields improves the representation of the whole chemical system and thus reduces the model–observation mismatch arising from non-LNO<sub>x</sub> sources and chemical processes. Therefore, this approach has the potential to improve global estimates of LNO<sub>x</sub> sources when compared to previous top-down approaches that optimize LNO<sub>x</sub> sources only. In this study, CHASER-DAS is utilized to assimilate multiple satellite datasets in order to analyze the global LNO<sub>x</sub> sources, including the vertical profiles, for the whole year 2007.

The rest of this paper is structured as follows: Sect. 2 describes the observations used for assimilation and validation. Section 3 introduces the data assimilation system. Section 4 presents the results of the global LNO<sub>x</sub> source estimation. Section 5 presents the regional LNO<sub>x</sub> structure over the Pacific and central Africa. Section 6 discusses the possible errors in the source estimation and the implications for the lightning parameterizations. Section 7 summarizes this study.

## 2 Data

### 2.1 Assimilated data

As depicted in Fig. 1, the LNO<sub>x</sub> source is estimated from a simultaneous assimilation of NO<sub>2</sub>, O<sub>3</sub>, CO, and HNO<sub>3</sub> retrievals from satellite measurements by the Ozone Monitoring Instrument (OMI), Tropospheric Emission Spectrometer (TES), Microwave Limb Sounder (MLS), and Measurement of Pollution in the Troposphere (MOPITT) instruments. The observation operator,

$$y = H(x) = x_a + \mathbf{A}(S(x) - x_a), \quad (1)$$

is constructed on the basis of the spatial interpolation operator ( $S$ ), the a priori profile ( $x_a$ ) and the averaging kernel ( $\mathbf{A}$ ), which maps the model fields ( $x$ ) into observation space ( $y$ ) while taking into account the vertical averaging implicit in the observations.

This section describes the observations, with a focus on the application of LNO<sub>x</sub> source estimation. More extended descriptions of the observations, their quality, and the filtering method used in CHASER-DAS are provided in Miyazaki et al. (2012a). Figure 1 shows how the individual satellite datasets provide information on different aspects of the chemical system in the middle and upper troposphere. Combined, these instruments provide strong constraints on LNO<sub>x</sub>. The contributions from the individual satellite sensors are highlighted below.

## Lightning NO<sub>x</sub> production estimation

K. Miyazaki et al.

Title Page

Abstract

Introduction

Conclusions

References

Tables

Figures

◀

▶

◀

▶

Back

Close

Full Screen / Esc

Printer-friendly Version

Interactive Discussion



## 2.1.1 OMI NO<sub>2</sub>

Tropospheric NO<sub>2</sub> column retrievals obtained from the version-2 OMI DOMINO data product (Boersma et al., 2011) are used to constrain the LNO<sub>x</sub> sources, the surface emissions of NO<sub>x</sub>, and the concentrations of NO<sub>y</sub> species. The overpass time of OMI (13:30) is more suitable for LNO<sub>x</sub> source estimation than the morning time observation by other satellite instruments (GOME, GOME-2, and SCIAMACHY), because lightning activity over land is strongest in the late afternoon and very weak in the morning (e.g. Lay et al., 2007). We employ the super observation approach to produce representative data with a horizontal resolution of 2.5° × 2.5°, following Miyazaki et al. (2012b). This approach avoids complications caused by the small (13–24 km) footprint of OMI at nadir. Therefore, the data assimilation adjusts the LNO<sub>x</sub> sources at grid scale rather than individually at OMI scale.

Boersma et al. (2005, 2011) summarized the general error characteristics of tropospheric NO<sub>2</sub> retrievals. For retrievals with small values, as over the oceans, the uncertainty is dominated by the combined error from spectral fitting and stratospheric column estimation. For columns exceeding  $0.5 \times 10^{15}$  molec cm<sup>-2</sup>, as over most continents, the uncertainty grows due to increasing errors related to cloud fraction, albedo, and profile shape. Clouds have a large influence on the errors and sensitivity in the measurements of the retrieved columns. Clouds below an NO<sub>2</sub> layer increase the effective albedo of the scene and increase the detected slant column, whereas high clouds partly screen the NO<sub>2</sub> column below (Boersma et al., 2005). We employ both clear-sky data and cloud-scene data in the LNO<sub>x</sub> estimation because both are sensitive to NO<sub>2</sub> produced by lightning higher up in the atmosphere. For the cloud-covered observations the averaging kernel shows a sharp drop roughly halfway the cloud, and very small sensitivities below. The location and magnitude of the drop is based on the cloud fraction and effective top height retrieved from the observations.

Title Page

Abstract

Introduction

Conclusions

References

Tables

Figures



Back

Close

Full Screen / Esc

Printer-friendly Version

Interactive Discussion



## 2.1.2 TES O<sub>3</sub>

The TES O<sub>3</sub> retrievals used are the version-4 level-2 nadir data obtained in the global survey mode (Bowman et al., 2006). This product represents 16 orbits daily, with a horizontal resolution of 5–8 km. Its vertical resolution is typically 6 km, with sensitivity to both the lower and upper troposphere (Worden et al., 2004; Bowman et al., 2006; Jourdain et al., 2007). Jourdain et al. (2010) argued that the TES provides direct observations of ozone-enhanced layers downwind of convective events and thus is a valuable dataset for estimating the vertical LNO<sub>x</sub> profiles. This can be attributed to its high sensitivity to LNO<sub>x</sub> relevant altitude layers, typically with more than one degree of freedom (DOF) for the middle and upper troposphere (from 500 hPa to the tropopause).

## 2.1.3 MLS O<sub>3</sub>, HNO<sub>3</sub>

The version-3.3 level-2 MLS products for O<sub>3</sub> and HNO<sub>3</sub> (Livesey et al., 2011) are used to constrain the LNO<sub>x</sub> sources in the upper troposphere and the chemical concentrations in the upper troposphere and the lower stratosphere. We use data on O<sub>3</sub> and HNO<sub>3</sub> only for pressures lower than 215 hPa and 150 hPa, respectively, owing to data quality problems for higher pressures. Martin et al. (2007) demonstrated that O<sub>3</sub> and HNO<sub>3</sub> measurements by limb viewing spaceborne sounders have a great potential to constrain the LNO<sub>x</sub> sources in the upper troposphere, based on Atmospheric Chemistry Experiment Fourier Transform Spectrometer (ACE-FTS) measurements.

## 2.1.4 MOPITT CO

The MOPITT CO retrievals employed are the version-5 level-2 thermal-infrared (TIR) data (Deeter et al., 2011, 2013). These observations are used for optimizing the surface CO emissions and the concentrations of CO and non-methane hydrocarbons (NMHCs). However, the covariances between the CO observations and the NO<sub>x</sub> sources are neglected in the analysis, since the error correlations are not expected to

### Lightning NO<sub>x</sub> production estimation

K. Miyazaki et al.

[Title Page](#)[Abstract](#)[Introduction](#)[Conclusions](#)[References](#)[Tables](#)[Figures](#)[⏪](#)[⏩](#)[◀](#)[▶](#)[Back](#)[Close](#)[Full Screen / Esc](#)[Printer-friendly Version](#)[Interactive Discussion](#)

contain meaningful information, and the limited ensemble size creates spurious correlations between non- or weakly-related variables (see Sect. 3.1.2). Even so, the CO observations indirectly affect the LNO<sub>x</sub> source estimation through their influence on the oxidation capacity and the NO<sub>x</sub> chemistry.

## 2.2 Validation data

Independent ozone observations are used to validate the performance of the data assimilation. The spatial distribution of tropospheric O<sub>3</sub> in the tropics is validated against the monthly mean tropospheric ozone column (TOC) derived using the OMI total columns and the MLS profiles from Ziemke et al. (2006) with a horizontal resolution of 1° × 1.25°. Ozonesonde observations taken from the database of the the Southern Hemisphere Additional Ozonesondes (SHADOZ) project (Thompson et al., 2007) are used to validate the vertical profile of O<sub>3</sub> in the troposphere and the lower stratosphere. The validation is performed at four sites in different regions of the tropics: Costa Rica in central America (10° N, 84° W), Irene in South Africa (25.9° S, 28.2° E), Pago Pago in American Samoa (14.4° S, 170.6° W), and San Cristobal in Ecuador (0.9° S, 89.6° W). For the purpose of comparison, all ozonesonde profiles are interpolated to a common vertical pressure grid with a cell size of 25 hPa. The model profiles are linearly interpolated to the location and time of each observation point.

## 3 Methodology

### 3.1 Data assimilation system

CHASER-DAS has been developed for the analysis of chemical compounds in the troposphere (Miyazaki et al., 2012a, b; Miyazaki and Eskes, 2013). This system simultaneously optimizes the LNO<sub>x</sub> sources and surface emissions of NO<sub>x</sub> and CO as well as the predicted concentrations of 35 chemical species. With the assimilation of

## Lightning NO<sub>x</sub> production estimation

K. Miyazaki et al.

Title Page

Abstract

Introduction

Conclusions

References

Tables

Figures

◀

▶

◀

▶

Back

Close

Full Screen / Esc

Printer-friendly Version

Interactive Discussion



data on multiple species, an improved description of the chemical interactions can be obtained, especially in relation to the  $\text{NO}_x\text{-CO-OH-O}_3$  set of chemical reactions.

Miyazaki and Eskes (2013) demonstrated that multi-species data assimilation improves the analysis of surface  $\text{NO}_x$  emissions, in comparison with an inversion derived from  $\text{NO}_2$  measurements alone. They showed that the assimilation of measurements for species other than  $\text{NO}_2$  changes the regional estimates of monthly mean surface  $\text{NO}_x$  by up to  $-58\%$  to  $+32\%$ . These large changes emphasize that uncertainties in the model chemistry affect the quality of the emission estimates. Similar benefits may be expected from the multi-species data assimilation to improve the  $\text{LNO}_x$  source estimation through corrections made to the concentrations of various chemical species. This is especially true for  $\text{LNO}_x$ , because all satellite sensors are sensitive in the altitude range where  $\text{LNO}_x$  and the ozone produced by  $\text{LNO}_x$  resides, see Fig. 1.

### 3.1.1 A global chemical transport model CHASER

The forecast model used is the global CTM CHASER (Sudo et al., 2002), which describes chemical and transport processes in the troposphere. The model has a so-called T42 horizontal resolution ( $2.8^\circ$ ) and 32 vertical levels from the surface to 4 hPa. CHASER is coupled to the atmospheric general circulation model (AGCM) version 5.7b of the Center for Climate System Research and Japanese National Institute for Environmental Studies (CCSR/NIES). At each time step of the model, the AGCM fields are nudged toward the reanalysis (Kanamitsu et al., 2002) by the Atmospheric Model Inter-comparison Project II of the National Centers for Environmental Prediction and US Department of Energy (NCEP-DOE/AMIP-II). Hence, the model realistically reproduces large-scale circulation while simulating sub-grid-scale convection using the cumulus convection parameterization (Arakawa and Schubert, 1974; Pan and Randall, 1998).

Anthropogenic  $\text{NO}_x$  emissions are based on the Emission Database for Global Atmospheric Research (EDGAR) version 4.2. Emissions from biomass burning are based on the Global Fire Emissions Data base (GFED) version 3.1 (van der Werf et al., 2010). Emissions from soils are based on monthly mean Global Emissions Inventory Activity

(GEIA) (Graedel et al., 1993). A diurnal variability scheme is implemented for the surface  $\text{NO}_x$  emissions, depending on the dominant category for each emission category (Miyazaki et al., 2012b). The total  $\text{NO}_x$  emission by aircraft is obtained from EDGAR as  $0.55 \text{ Tg N yr}^{-1}$ .

### 5 3.1.2 Local ensemble transform Kalman filter

The data assimilation technique employed is local ensemble transform Kalman filter (Hunt et al., 2007). In the forecast step, a background ensemble,  $\mathbf{x}_i^b (i = 1, \dots, k)$ , is globally obtained from the evolution of each ensemble model realisation, where  $\mathbf{x}$  represents the model variable;  $b$  the background state; and  $k$  the ensemble size. In the analysis step, an ensemble of background observation vectors in the observation space,  $\mathbf{y}_i^b = H(\mathbf{x}_i^b)$ , is estimated using the observation operator  $H$ . A background ensemble mean in the observation space,  $\overline{\mathbf{y}^b} = \frac{1}{k} \sum_{i=1}^k \mathbf{y}_i^b$ , or in the model space,  $\overline{\mathbf{x}^b} = \frac{1}{k} \sum_{i=1}^k \mathbf{x}_i^b$ , and an ensemble of background perturbations in the observation space,  $\mathbf{Y}^b = \mathbf{y}_i^b - \overline{\mathbf{y}^b}$ , or in the model space,  $\mathbf{X}^b = \mathbf{x}_i^b - \overline{\mathbf{x}^b}$ , are also computed. The ensemble mean is then updated by

$$\overline{\mathbf{x}^a} = \overline{\mathbf{x}^b} + \mathbf{X}^b \tilde{\mathbf{P}}^a (\mathbf{Y}^b)^T \mathbf{R}^{-1} (\mathbf{y}^o - \overline{\mathbf{y}^b}), \quad (2)$$

where  $\mathbf{y}^o$  is the observation vector, and  $\mathbf{R}$  is the  $p \times p$  observation error covariance ( $p$  is the number of observation).  $\tilde{\mathbf{P}}^a$  is the local analysis error covariance in the ensemble space,

$$\tilde{\mathbf{P}}^a = \left[ (k-1)I + (\mathbf{Y}^b)^T \mathbf{R}^{-1} \mathbf{Y}^b \right]^{-1}. \quad (3)$$

The new analysis ensemble perturbation matrix in the model space  $\mathbf{X}^a$  is obtained by transforming the background ensemble  $\mathbf{X}^b$ ,

$$\mathbf{X}^a = \mathbf{X}^b \left[ (k-1) \tilde{\mathbf{P}}^a \right]^{1/2}. \quad (4)$$

## Lightning $\text{NO}_x$ production estimation

K. Miyazaki et al.

Title Page

Abstract

Introduction

Conclusions

References

Tables

Figures

◀

▶

◀

▶

Back

Close

Full Screen / Esc

Printer-friendly Version

Interactive Discussion



**Lightning NO<sub>x</sub>  
production  
estimation**

K. Miyazaki et al.

Title Page

Abstract

Introduction

Conclusions

References

Tables

Figures

◀

▶

◀

▶

Back

Close

Full Screen / Esc

Printer-friendly Version

Interactive Discussion



The new background error covariance used in the next forecast step is obtained from an ensemble simulation with the analysis ensemble. In the analysis, a covariance localization was applied to neglect the covariance among non- or weakly-related variables. For the optimization of LNO<sub>x</sub> sources, the covariances with TES O<sub>3</sub>, OMI NO<sub>2</sub>, MLS O<sub>3</sub>, and MLS HNO<sub>3</sub> observations are considered, while those with MOPITT CO data are not. MOPITT CO data affect the concentrations of CO, hydrocarbons, and formaldehyde only. Surface emissions of NO<sub>x</sub> and CO are optimized using OMI NO<sub>2</sub> data and MOPITT CO data, respectively (see Miyazaki et al., 2012a, for details). The covariance localization helps to avoid sampling errors resulting from the limited ensemble size and to improve the LNO<sub>x</sub> analysis.

The localization is also applied to avoid the influence of remote observations for improving the filter performance. The influence of an observation is cut off when the distance between the observation and an analysis point is larger than  $2L \times \sqrt{10/3}$  based on the formulation of Gaspari and Cohn (1999). The localization scale  $L$  is 600 km in our setting. As a result, the analysis is solved at every grid point by choosing nearby observations. The emission and concentration fields are updated at an analysis interval of every 100 min, with the ensemble size of 48. Further details are described in Miyazaki et al. (2012a).

## 3.2 LNO<sub>x</sub> estimation

### 3.2.1 Parameterization

Lightning is routinely monitored from ground-based networks and detected from satellite instruments. Nevertheless, these data cannot be directly used in CTM simulations, because of the very small amount of global coverage on a daily basis. Thus, a parameterization is required in order to estimate the lightning flash frequency in CTM simulations. The global distribution of the flash rate is calculated in CHASER on the basis of the observed relation between the lightning activity and the cloud top height

Lightning NO<sub>x</sub>  
production  
estimation

K. Miyazaki et al.

Title Page

Abstract

Introduction

Conclusions

References

Tables

Figures

◀

▶

◀

▶

Back

Close

Full Screen / Esc

Printer-friendly Version

Interactive Discussion



(Price and Rind, 1992) in the AGCM at each forecast step. In this approach, high clouds are expected to exhibit strong lightning activity. The frequencies of lightning over the continents and the oceans are estimated separately as follows (Price et al., 1997):  $F_c = 3.44 \times 10^{-5} \times H^{4.92}$  (flashes  $\text{min}^{-1}$ ) over continents;  $F_m = 6.40 \times 10^{-4} \times H^{1.73}$  (flashes  $\text{min}^{-1}$ ) over ocean, where  $F$  is the total flash rate (flashes  $\text{min}^{-1}$ ) and  $H$  is the cloud top height (km), in which a globally and annually constant tuning factor is applied for the total flash frequency in CHASER simulations.

The simulated average global flash rate for 2007 is  $41.2 \text{ flashes s}^{-1}$ , which is comparable to the climatological estimates of  $44 \pm 5 \text{ flashes s}^{-1}$  derived from the Optical Transient Detector (OTD) measurements (Christian et al., 2003). The simulated global flash rate shows a maximum in boreal summer and a minimum in boreal winter, with frequent occurrences over Central Africa, South America, and the maritime continent. These features are commonly found in the climatological observations. Conversely, in comparison with the observed flash activity, the simulated flash activity is stronger over South America but weaker over central Africa and most of the oceanic ITCZ. These systematic differences found in studies using the scheme of Price and Rind (1992) have been reported before (e.g. Allen and Pickering, 2002; Labrador et al., 2005; Martin et al., 2007).

The LNO<sub>x</sub> source is estimated at each grid point of CHASER by using the simulated lightning activity and making several assumptions. First, the ratio  $z$  between the IC flashes and CG flashes is estimated as a function of the cold cloud thickness ( $\Delta H$  for  $< 0^\circ\text{C}$ ) on the basis of the following relationship (Price et al., 1997):

$$z = 0.021 \times \Delta H^4 - 0.648 \times \Delta H^3 + 7.493 \times \Delta H^2 - 36.54 \times \Delta H + 63.09. \quad (5)$$

This relationship is applied for clouds with  $\Delta H > 5.5 \text{ km}$ , while  $z$  is set to zero for clouds with  $\Delta H < 5.5 \text{ km}$  based on the observation that low clouds almost exclusively have IC flashes during the growth stage. Second, the LNO<sub>x</sub> source amounts are calculated on the basis of a lightning NO production of 1100 moles per CG flash and 110 moles per IC flash, with a mean energy per CG flash of  $6.7 \times 10^9 \text{ J flash}^{-1}$  (Price et al.,

1997). Third, the vertical profiles of the LNO<sub>x</sub> sources are determined on the basis of the C-shaped profile given by Pickering et al. (1998), with a first maximum in the upper troposphere and a second maximum in the lower troposphere. The global annual total amount of the LNO<sub>x</sub> source for 2007 was estimated at 4.7 TgNyr<sup>-1</sup> in the CHASER simulations.

### 3.2.2 Optimization by data assimilation

The multiplication factors for the LNO<sub>x</sub> production rate (mol s<sup>-1</sup>) and the NO<sub>x</sub> surface emissions are optimized in the assimilation analysis step, by adding them to the state vector together with the forecast variables (i.e. concentrations). In this approach, the background error covariance matrix estimated from the ensemble simulations is used to obtain best estimates of the source factors at each grid point of the model. Figure 2 shows the mean background error covariance structure between the LNO<sub>x</sub> source and the concentrations of various species at different altitudes over central Africa in July. The concentrations of chemical species such as O<sub>x</sub>, NO<sub>x</sub>, N<sub>2</sub>O<sub>5</sub>, HNO<sub>3</sub>, HNO<sub>4</sub> exhibit high positive correlations with the LNO<sub>x</sub> sources in the middle and upper troposphere. The high correlations indicate the utility of measurements of these species to constrain the LNO<sub>x</sub> sources. The background error covariance varies in time and space in the EnKF approach, reflecting variations in the lightning activity and the chemical concentrations.

In order to provide meaningful constraints on LNO<sub>x</sub>, the observation error of each retrieval must be sufficiently small compared to lightning signal. As shown in Fig. 3, the CHASER simulations with and without the lightning signal in the tropospheric NO<sub>2</sub> columns gives the magnitude of the boreal summer (June–August) mean lightning signal as roughly  $1 \sim 5 \times 10^{14}$  molec cm<sup>-2</sup> over the tropical Atlantic, Africa, and India but roughly  $1 \times 10^{14}$  molec cm<sup>-2</sup> over remote land sites. The large enhancements are over, and downwind of, active convective regions (e.g. over the tropical Atlantic), as found by Martin et al. (2007). These signals are large compared to the local super-observation error of the OMI retrievals, in which the total super observation error is

## Lightning NO<sub>x</sub> production estimation

K. Miyazaki et al.

Title Page

Abstract

Introduction

Conclusions

References

Tables

Figures

◀

▶

◀

▶

Back

Close

Full Screen / Esc

Printer-friendly Version

Interactive Discussion



## Lightning NO<sub>x</sub> production estimation

K. Miyazaki et al.

Title Page

Abstract

Introduction

Conclusions

References

Tables

Figures



Back

Close

Full Screen / Esc

Printer-friendly Version

Interactive Discussion



computed as a combination of the measurement error and the representativeness error as in Miyazaki et al. (2012b). The superobservation error is relatively small because of the large number of OMI observations per grid cell. Large enhancements in O<sub>3</sub> due to lightning are observed in the tropical upper troposphere, with contributions as large as 13 ppbv to the mean concentration, consistent with the analyses of Cooper et al. (2006) and Hudman et al. (2007). These signals are slightly less than or nearly equal to the mean TES observation error. The mean MLS observation errors are generally much larger than the lightning signals, especially for HNO<sub>3</sub>. Although the mean ratio of the lightning signals to the retrieval error is small, a large number of observations can still provide constraints on LNO<sub>x</sub> estimates.

The observed concentrations reflect contributions not only from LNO<sub>x</sub> but also from other sources such as surface emissions and inflows from the stratosphere. Any model errors in the other sources will produce model–observation mismatches that will negatively affect the accuracy of the estimated LNO<sub>x</sub> source in the top down framework. To avoid difficulties related to contributions from surface sources, for instance, Boersma et al. (2005) focused on situations downwind of storm systems over areas relatively free of pollution. In contrast, our analysis simultaneously corrects the various model error sources, which benefits the LNO<sub>x</sub> source analysis even over polluted regions. Moreover, the combined use of the multiple datasets with different vertical sensitivities is expected to facilitate the estimation of the vertical LNO<sub>x</sub> profile and to distinguish between the surface NO<sub>x</sub> emissions and LNO<sub>x</sub> sources. The MLS and TES data not only provide information on the NO<sub>x</sub> source amount in the middle and upper troposphere, but also constrain the the lower tropospheric source when combined with the OMI tropospheric column NO<sub>2</sub> retrievals.

The a priori error is set to 40 % for the surface emissions of NO<sub>x</sub> and CO and 60 % for the LNO<sub>x</sub> sources, considering the large uncertainties in the lightning parameterization. Since no model error term is implemented for the source factors during the forecast step, the background error covariance may continuously decrease and become underestimated through the data assimilation cycle. Thus, we apply covariance infla-

tion to the source factors to prevent covariance underestimation in the analysis step, as was done for the surface emission in Miyazaki et al. (2012a). The standard deviation is artificially inflated to a minimum predefined value (i.e., 30 % of the initial standard deviation) at each analysis step for both the surface and lightning sources. The sensitivity of the analysis to the choice of these parameters is discussed in Sect. 6.2.

## 4 Results

### 4.1 Global LNO<sub>x</sub> source distributions

Data assimilation increases the global annual LNO<sub>x</sub> source from 4.7 to 6.3 Tg Nyr<sup>-1</sup>, as summarized in Table 1. The instantaneous uncertainty estimated from the mean analysis spread for the global source is ±0.9 Tg Nyr<sup>-1</sup>, while the chi-square ( $\chi^2$ ) diagnostic gives confidence in the estimated analysis spread as a measure of the analysis uncertainty (c.f., Sect. 6.1.3). This spread of the ensemble is relatively small, showing that LNO<sub>x</sub> is well constrained by the assimilation. The Northern Hemisphere (NH, 20–90° N), the tropics (20° S–20° N), and the Southern Hemisphere (SH, 90–20° S) contribute 31 %, 56 %, and 13 % to the analyzed global source, respectively. These relative contributions are slightly modified from the a priori sources. The analyzed global source is maximal in July, primarily resulting from the seasonal variation in the NH, as depicted in Fig. 4.

Figure 5 compares the simulation with the assimilation in terms of the global distribution of annual total LNO<sub>x</sub> sources. Data assimilation substantially increases the annual sources over central Africa, the central and eastern United States, northern Eurasia, South America, south and southeast Asia, the maritime continent, and over the tropical oceans around the ITCZ (left panels). The seasonal amplitudes are also enhanced by 10–40 % over most of these regions (middle panels). Data assimilation introduces distinct seasonal variations in sources over the oceans, especially along the ITCZ. The maximum LNO<sub>x</sub> sources mostly appear in June or July over the NH temperate regions

## Lightning NO<sub>x</sub> production estimation

K. Miyazaki et al.

[Title Page](#)[Abstract](#)[Introduction](#)[Conclusions](#)[References](#)[Tables](#)[Figures](#)[◀](#)[▶](#)[◀](#)[▶](#)[Back](#)[Close](#)[Full Screen / Esc](#)[Printer-friendly Version](#)[Interactive Discussion](#)

and in December or January over the SH continents (right panels). Compared to those over most other NH regions, the peak sources over northern Africa and India occur 1–2 months later (i.e., in July–August), reflecting the local convective activity during the African and Asian monsoons, respectively. The timing of the peak sources is very similar between the simulation and the assimilation, because the seasonal variation of the lightning flash frequency is generally well predicted by the model as compared with the OTD climatology (figure not shown). However, data assimilation changes the peak time by 1–2 months over central Africa and South America.

## 4.2 Regional LNO<sub>x</sub> source distributions

Figure 6 shows the seasonal variations of the LNO<sub>x</sub> source over the 11 regions shown in the top panel. Over the NH continents (e.g. North America, Europe, and northern Eurasia), the broad summertime source peak is predicted by the model, where the monthly peak source strength is further increased by 30–60 % due to assimilation. Over northern Eurasia, the large increase in the summer dominates the approximately 40 % increase in the annual total source. The relative increase is more constant with season over Europe.

The seasonal variations of the sources differ significantly among the regions in the tropics, reflecting the locality of convection and monsoon activity. The predicted sources exhibit broad maxima in the rainy seasons over the tropical continental regions; that is, from October to April over South America, from April to September over Northern Africa, and from May to September over Southeast Asia. Data assimilation generally enhances the seasonality of the tropical sources, e.g. producing two source maxima in May and July over northern Africa. The sources over South America are increased by about 40 % from October to February, which is primarily attributed to enhanced sources over the Amazon during the South American monsoon.

Over the oceans, the retrieval uncertainties of OMI, TES, and MOPITT measurements are generally larger compared to over land. Nevertheless, substantial changes in the regional LNO<sub>x</sub> sources are obtained by assimilation over the Pacific, the Indian

Title Page

Abstract

Introduction

Conclusions

References

Tables

Figures



Back

Close

Full Screen / Esc

Printer-friendly Version

Interactive Discussion



Ocean, and the Atlantic in the tropics, especially along the ITCZ, because of large lightning signals in the chemical concentrations. Data assimilation produces obvious source maxima in boreal late winter over the Atlantic and in boreal autumn–early winter over the Indian Ocean. The west African and south Asian monsoons, respectively, may be responsible for these enhancements where the model failed to predict the distinct seasonality. The LNO<sub>x</sub> sources over the tropical Pacific are largely increased throughout the year, with a mean factor of about two. As a result, the data assimilation increases the annual global source by about 56 % over the oceans. The relative increase of the total source is smaller over land (i.e., 32 %) than over the oceans.

### 4.3 Vertical distribution of the LNO<sub>x</sub> source

Figure 7 shows the changes in the vertical profiles of the LNO<sub>x</sub> sources. Data assimilation increases the LNO<sub>x</sub> sources over most land regions by 20–50 % in the upper troposphere, with a maximum increase at 240 hPa in the global and annual mean. The corrections below the middle troposphere are much smaller. Compared to other land regions, the source increase in the upper troposphere is much smaller over Australia. Over the oceans, persistent strong sources associated with the simulated low clouds and the occurrence of IC flashes are predicted in the lower troposphere. Data assimilation further increases the lower tropospheric sources by a factor of up to two. A roughly twofold increase in the upper tropospheric sources occurs over the Pacific. In the annual and global mean, the LNO<sub>x</sub> sources over the oceans are increased by 40–50 % in the lower troposphere and by up to 65 % in the upper troposphere.

Table 2 summarizes the altitude (in km) with maximum LNO<sub>x</sub> emission (i.e., source peak height). The predicted source peak heights of the regional sources over land mostly range from 5 km to 12 km but exceed 13 km locally over central Africa and central America. Data assimilation generally lowers the regional mean peak source heights, with large decreases at low latitudes over land. Substantial decreases in the peak heights of the annual sources occur over Southeast Asia (–0.74 km), Australia (–0.41 km), and southern Africa (–0.38 km), whereas the changes are small over North

America and northern Eurasia. Over the oceans, and in particular over the tropical western Pacific, the peak height is substantially lowered by about 1.2 km.

#### 4.4 Relative contributions of individual assimilated datasets

The effects of individual assimilated datasets on the estimated LNO<sub>x</sub> sources were evaluated through observing system experiments (OSEs) by separately assimilating each dataset with CHASER-DAS (Fig. 8). The assimilation of OMI NO<sub>2</sub> measurements dominates the overall structure of the total analysis increment. The spatial distribution in the monthly mean analysis increment of the source column reveals a high correlation between the full assimilation and the OSE with OMI measurements ( $r = 0.55\text{--}0.60$ ). This demonstrates the dominant role of the OMI NO<sub>2</sub> retrievals in determining the LNO<sub>x</sub> source distribution in the analysis.

The measurements of species other than NO<sub>2</sub> also provide important constraints on the global source estimation. The assimilated datasets all have an impact on the global source analysis, but with different contributions from individual datasets, as summarized in Table 3. The vertical and latitudinal structure of the analysis increments obtained from the assimilation of MLS O<sub>3</sub> and HNO<sub>3</sub> data are generally similar (Fig. 8), revealing consistent constraints from datasets gathered for different species but with the same instrument. In contrast, the respective corrections from MLS O<sub>3</sub> and TES O<sub>3</sub> measurements show differences in magnitude and distribution. This arises from differences between the two sets of measurements in the coverage, vertical sensitivity, and systematic error. The negative analysis increments in the upper tropospheric LNO<sub>x</sub> sources obtained from the assimilation of TES O<sub>3</sub> data likely arises from the TES negative bias (up to 20%) from the upper troposphere to the lower stratosphere, see e.g. Nassar et al. (2008).

The influences measured by the OSEs mostly reflect the effect of direct source optimization through the background error covariance. In addition, each retrieval indirectly affects the source estimation through adjustments made to the various concentration fields. For instance, the assimilation of the MLS retrievals corrects the concentrations

### Lightning NO<sub>x</sub> production estimation

K. Miyazaki et al.

Title Page

Abstract

Introduction

Conclusions

References

Tables

Figures



Back

Close

Full Screen / Esc

Printer-friendly Version

Interactive Discussion



of O<sub>3</sub> and NO<sub>y</sub> species in the stratosphere, which has the potential to improve the modelled impact of stratospheric air on tropospheric concentrations and benefits the source estimate derived from tropospheric column. Furthermore, the assimilation of MOPITT CO data changes the free tropospheric OH concentration by up to 5 %, corresponding to an increase of about 25 % in the annual NH total CO emissions (Miyazaki et al., 2012a), which changed the monthly global LNO<sub>x</sub> source by up to 5 % in combination with the other satellite datasets.

In most previous studies, NO<sub>2</sub> measurements were used to optimise only the LNO<sub>x</sub> production. In this case, the accuracy of the LNO<sub>x</sub> source estimates is negatively affected by various sources of error, including the surface NO<sub>x</sub> and CO emissions and inflows from the stratosphere. We found differences reaching about 50 % on the regional scale when comparing the multi-species assimilation and a simpler LNO<sub>x</sub> source (i.e. single-parameter) inversion derived from NO<sub>2</sub> measurements only. The single-parameter approach tends to have larger sources (e.g., the estimated global LNO<sub>x</sub> source was 8.89 TgNyr<sup>-1</sup> for January and 12.8 TgNyr<sup>-1</sup> for July), because of the analysis increment introduced to compensate for other sources of error. Miyazaki and Eskes (2013) showed that the a priori surface NO<sub>x</sub> emissions are possibly underestimated by up to 67 % on the regional scale. The simulated O<sub>3</sub> concentrations in the stratosphere are also biased (Miyazaki et al., 2012a). These sources of error leads to an excessive model–observation mismatch in the LNO<sub>x</sub> source inversion. Note that, because of the short assimilation cycle (i.e., 100 min.), the LNO<sub>x</sub> source can be frequently and continuously increased to compensate for persistent model errors. This situation may cause larger LNO<sub>x</sub> sources in our estimates compared to those with a longer (e.g., one month) assimilation cycle especially when only LNO<sub>x</sub> sources are optimized.

## Lightning NO<sub>x</sub> production estimation

K. Miyazaki et al.

[Title Page](#)[Abstract](#)[Introduction](#)[Conclusions](#)[References](#)[Tables](#)[Figures](#)[⏪](#)[⏩](#)[◀](#)[▶](#)[Back](#)[Close](#)[Full Screen / Esc](#)[Printer-friendly Version](#)[Interactive Discussion](#)



## Lightning NO<sub>x</sub> production estimation

K. Miyazaki et al.

Title Page

Abstract

Introduction

Conclusions

References

Tables

Figures

⏪

⏩

◀

▶

Back

Close

Full Screen / Esc

Printer-friendly Version

Interactive Discussion



and high convective available potential energy (CAPE) activate vertical uplifting and lightning. The parameterization for the flash rate estimation assumes that the meteorological fields in the model represent the deep convection that generates lightning. Large uncertainties in the simulated clouds and the LNO<sub>x</sub> sources are expected over the tropical western Pacific, since these are heavily parameterized in the model.

Figure 10 shows the regional distribution of total cloud fraction and tropospheric concentrations of NO<sub>2</sub> and O<sub>3</sub> over the tropical western Pacific in mid-August. Compared to the OMI cloud data, the GCM shows systematic errors in the location and total cloud fraction of the ITCZ. Although the meteorological conditions in the GCM are nudged toward the NCEP-II reanalysis, the use of the cumulus parameterization causes a large uncertainty in the simulated cloud and LNO<sub>x</sub> source structures. The regional mean strength of the LNO<sub>x</sub> sources is increased by a factor of two due to data assimilation, but the spatial distribution is only slightly modified because of the sparse coverage of the observations and large uncertainty in individual data.

The simulation underestimates the regional mean NO<sub>2</sub> concentration in the upper troposphere by 65% compared to the OMI NO<sub>2</sub> retrieval, whereas data assimilation removes most of the bias. Agreements with TES O<sub>3</sub> fields are also greatly improved by data assimilation, despite the sparse coverage of the TES measurements. Because of the simultaneous optimization of the LNO<sub>x</sub> sources and these chemical concentrations, the improvements suggest that the regional total LNO<sub>x</sub> sources are reasonably estimated by data assimilation. In contrast, to better represent the observed fine structure associated with individual occurrences of cloud, a high-resolution model is required. This is discussed further in Sect. 6.1.2.

### 5.3 Central Africa

Africa is the region with the strongest lightning activity and the largest source of biomass burning over the globe (e.g. Christian et al., 2003). In this region, large uncertainties in the simulated cumulus cloud and biomass burning activity are expected, which will cause errors in the predicted LNO<sub>x</sub> sources and chemical concentrations.

## Lightning NO<sub>x</sub> production estimation

K. Miyazaki et al.

Title Page

Abstract

Introduction

Conclusions

References

Tables

Figures

◀

▶

◀

▶

Back

Close

Full Screen / Esc

Printer-friendly Version

Interactive Discussion



NO<sub>2</sub> concentrations exhibit distinct vertical and latitudinal variations over western Africa (Fig. 11). These variations are produced by various factors such as convective uplifting, stratospheric inflows, surface sources, and lightning sources. The lower tropospheric NO<sub>2</sub> concentrations are maximal over northern (around 5–20° N) and central (153° S–

5 Equator) Africa, owing to in situ emissions from biomass burning. In the upper troposphere, strong LNO<sub>x</sub> sources cause a maximum NO<sub>2</sub> concentration over northern Africa (5–15° N). Data assimilation increases the surface NO<sub>x</sub> emissions over northern and central Africa by up to 90 % and the LNO<sub>x</sub> source over northern Africa by about 50 %, which acts to strengthen the local maximum in NO<sub>2</sub> concentrations.

10 The tropospheric O<sub>3</sub> distributions also show distinct variations over central Africa. The surface NO<sub>x</sub> and CO emissions and LNO<sub>x</sub> sources lead to O<sub>3</sub> production, whereas the inflows from the stratosphere along the subtropical jet stream predominantly determine the latitudinal O<sub>3</sub> variations in the upper troposphere. The multi-species data assimilation provides comprehensive constraints on these processes and the O<sub>3</sub> variations.

15 The assimilation of TES data modifies the O<sub>3</sub> distribution around the African monsoon circulation, whereas the assimilation of MLS observations improves the stratospheric inflow. Assimilation of MOPITT and OMI measurements provides important constraints on the OH fields and chemical O<sub>3</sub> production. These case studies demonstrate once more the utility of the simultaneous data assimilation for regional process

20 studies.

## 6 Discussion

### 6.1 Uncertainty of the LNO<sub>x</sub> source estimate

#### 6.1.1 Systematic satellite observation errors

25 The quality of the assimilated measurements largely influences the LNO<sub>x</sub> source uncertainty. Boersma et al. (2011) showed that the different OMI NO<sub>2</sub> retrievals have biases

**Lightning NO<sub>x</sub>  
production  
estimation**

K. Miyazaki et al.

Title Page

Abstract

Introduction

Conclusions

References

Tables

Figures

◀

▶

◀

▶

Back

Close

Full Screen / Esc

Printer-friendly Version

Interactive Discussion



up to 40 % because of errors in the retrieval processes. Although this study uses the latest improved retrievals, systematic errors will still be present in the retrievals. We performed a sensitivity experiment by adding an artificial positive bias of 15 % to the OMI NO<sub>2</sub> retrievals. This increased the monthly regional and global LNO<sub>x</sub> sources by up to 14 % and 3 %, respectively, as summarized in Table 5. Any bias in the measurements of species other than NO<sub>2</sub> also affects the quality of the sources estimated in the simultaneous assimilation framework. TES O<sub>3</sub> data are known to have positive biases in the upper troposphere compared to ozonesonde observations (Worden et al., 2007; Nassar et al., 2008). A sensitivity experiment was performed in which a bias correction for TES O<sub>3</sub> data was applied. This consisted of a uniform 3.3 ppbv above 500 hPa and 6.5 ppbv below 500 hPa, as recommended by Worden et al. (2009). The result of this experiment suggests that such a bias in TES O<sub>3</sub> increases the estimated monthly global LNO<sub>x</sub> source by up to 14 % (Table 5). Implementing a reasonable bias correction scheme for individual retrievals is therefore clearly important to obtain unbiased source estimates.

The presence of clouds influences both the quality and sensitivity of the satellite retrievals. The retrieval uncertainty is increased by errors related to cloud fraction, while the retrieval sensitivity at cloud top or above is enhanced by multiple scattering and the high albedo (Boersma et al., 2005). In situations of high cloud with strong lightning activity, a large fraction of the LNO<sub>x</sub> reaches the top and anvil of the cloud (Ridley et al., 1996). The LNO<sub>x</sub> produced can reside above the cloud for several days, because of the long lifetime of NO<sub>x</sub> in the upper troposphere, and the enhanced concentrations may be detected by remote observations. Furthermore, an instrument like OMI is sensitive to NO<sub>2</sub> in the upper part of thunderstorm clouds. In most previous studies, however, cloud-covered observations were simply ignored to avoid anticipated retrieval complications. A sensitivity experiment was performed in which cloud-covered OMI NO<sub>2</sub> observations were removed when the cloud radiance fraction is larger than 50 %. This experiment confirmed that the cloud-covered data have an impact on the LNO<sub>x</sub> source estimation, as summarized in Table 5 and depicted in Fig. 12. The large changes associated with

## Lightning NO<sub>x</sub> production estimation

K. Miyazaki et al.

Title Page

Abstract

Introduction

Conclusions

References

Tables

Figures

◀

▶

◀

▶

Back

Close

Full Screen / Esc

Printer-friendly Version

Interactive Discussion



the cloud-covered data are found above roughly 450 hPa in the tropics and in the NH, with source increases up to about 40 % in the NH subtropical upper troposphere in July. The global LNO<sub>x</sub> source is increased by 12 % in July when cloud-covered observations are used. These results imply that cloud-covered OMI NO<sub>2</sub> data contain important information on the LNO<sub>x</sub> source amounts above and inside clouds. However, errors in the simulated cloud profiles (c.f., Fig. 10), and in the retrieved cloud-altitude dependent averaging kernels, may cause biases in the cloudy scene analysis.

The lifetimes of NO<sub>x</sub>, HNO<sub>3</sub>, and O<sub>3</sub> are much longer in the upper troposphere than in the lower troposphere, and also the satellite observations (e.g. TES, MLS, and cloud-covered OMI observations) show a higher sensitivity in the middle to upper troposphere. This situation also helps to provide constraints on the LNO<sub>x</sub> source far from the convective clouds that produced the LNO<sub>x</sub>. The large spread of the different estimates indicates that estimates of the LNO<sub>x</sub> source distribution and the global LNO<sub>x</sub> source amount are highly sensitive to the satellite data used. Subsequent use of new measurements is expected to influence the source estimation to a considerable degree.

### 6.1.2 Systematic model errors

The mismatch between the simulated and observed concentrations is partly caused by various sources of error in the model. For instance, errors in the lifetime of NO<sub>x</sub>, the emissions of ozone precursors, the inflows from the stratosphere, and the parameterization of convective transport will dominate the mismatch and thus may have an impact on the quality of the LNO<sub>x</sub> source estimation (e.g., Jourdain et al., 2010). As suggested in Sect. 4.4, the use of multiple datasets causes the analysis increment of the LNO<sub>x</sub> sources to become smaller because several sources of error are corrected simultaneously. In a parameter inversion that optimizes the LNO<sub>x</sub> sources only, the analysis increments will compensate for errors that occur not only in the LNO<sub>x</sub> sources but also in the other sources and species concentrations. This will result in overcorrections in the LNO<sub>x</sub> source estimation. Despite this advantage of the simultaneous assimilation

of multiple satellite datasets, sources of error will remain because the satellite data do not fully constrain the model. Possible systematic error sources are discussed below.

Cumulus convection plays an important role in determining the vertical profile of chemical concentrations. Because the  $\text{NO}_x$  chemical lifetime in the troposphere depends on altitude (i.e., longer at higher altitude), cumulus convection affects the total amount of  $\text{NO}_x$  in the troposphere and, accordingly,  $\text{NO}_x$  source inversion. However, the cumulus parameterization is highly uncertain and leads to systematic errors in the simulated clouds (e.g., Emori et al., 2005). A sensitivity experiment in which the convective mass flux from the cumulus parameterization was increased by 20 % resulted in a variation of up to 6 % in the tropical  $\text{LNO}_x$  sources (Table 5). The high sensitivity of the  $\text{LNO}_x$  source estimation to model convection is commonly reported by Lin (2012).

The model also shows systematic errors in the location of cumulus clouds (c.f., Fig. 10). An accurate determination of cloud positions is important for analysing the  $\text{LNO}_x$  source patterns. The location of the ITCZ clouds is sensitive to sea surface temperature (SST) in the GCM simulation. A sensitivity experiment using the SST data set obtained for 1997 (a strong El Niño year) showed a variation of up to 4 % in the global  $\text{LNO}_x$  estimates (Table 5) and increased the  $\text{LNO}_x$  sources over the Pacific by 14 % in January. This indicates that the uncertainty in the  $\text{LNO}_x$  estimate due to errors in the simulated clouds is significant.

The satellite measurements used in our analysis contain limited information to constrain the influences of model errors due to fast chemistry (e.g. which determines the  $\text{NO}_2/\text{NO}$  ratio) and transient transport processes (e.g. due to convection and boundary layer mixing). On the basis of a comparison with aircraft measurements, Miyazaki et al. (2012b) implied that the  $\text{NO}_2/\text{NO}$  ratio in the free troposphere over Mexico is not realistically represented even when observations of multiple species are assimilated. Accordingly, changes in the chemical scheme are expected to affect the estimated sources. For instance, Stavrakou et al. (2013) demonstrated the strong effect of  $\text{NO}_x$  loss uncertainties on top-down  $\text{NO}_x$  source inversion by using several different chemical schemes. In addition, the diurnal variations of lightning activity are determined

## Lightning $\text{NO}_x$ production estimation

K. Miyazaki et al.

Title Page

Abstract

Introduction

Conclusions

References

Tables

Figures

◀

▶

◀

▶

Back

Close

Full Screen / Esc

Printer-friendly Version

Interactive Discussion



## Lightning NO<sub>x</sub> production estimation

K. Miyazaki et al.

Title Page

Abstract

Introduction

Conclusions

References

Tables

Figures

◀

▶

◀

▶

Back

Close

Full Screen / Esc

Printer-friendly Version

Interactive Discussion



with the aid of the parameterization in the model, since the assimilated measurements provide constraints mainly around noon. Although the departures (observation minus forecast) reflect model errors accumulated over a period of several days, because of the long lifetime of the chemical constituents in the upper troposphere, errors in the simulated diurnal variability in the chemical concentrations and in the lightning activity will lead to large uncertainties in the source estimate.

The actual spatiotemporal scale of lightning activity is typically much smaller than the model resolution. A finer resolution model is required to capture the influences of lightning and atmospheric transport on the scale of individual clouds and efficiently assimilate fine-scale retrievals. We confirmed that in comparison with the GCM simulation the high-resolution Weather Research and Forecasting model (WRF-ARW) version 3.4.1 (Skamarock et al., 2008) with 3 km horizontal grid spacing and without any cumulus convection parameterization provides a better agreement with the satellite observations in terms of the cloud distribution over the western Pacific, by better representing the small-scale cloud and wind structures (figure not shown). Data assimilation with high-resolution models are expected to improve the LNO<sub>x</sub> source estimate.

### 6.1.3 Data assimilation error modelling

$\chi^2$  diagnostic tests (e.g. Menard and Chang, 2000) is used to measure the data assimilation statistics. The annual mean  $\chi^2$  was about 1.2 for OMI NO<sub>2</sub>, 0.8 for TES O<sub>3</sub>, 0.7 for MOPITT CO, 2.1 for MLS O<sub>3</sub>, and 1.6 for MLS HNO<sub>3</sub>, demonstrating that the overall magnitude of the background error covariances are reasonably modelled in the data assimilation. The too large  $\chi^2$  for the MLS data imply an overconfidence in the model, and is largely attributed to the prescribed concentrations for O<sub>3</sub>, NO<sub>x</sub>, HNO<sub>3</sub>, and N<sub>2</sub>O<sub>5</sub> above 20 km altitude in CHASER.

The mean analysis spread for the annual global source strength is about 0.9 Tg N yr<sup>-1</sup>. This can be translated into an error estimate for the total yearly source. The LNO<sub>x</sub> analysis is obtained from information of roughly two week of measurements, as demonstrated by the spin-up period of the assimilation. If we assume that individual



## Lightning NO<sub>x</sub> production estimation

K. Miyazaki et al.

Title Page

Abstract

Introduction

Conclusions

References

Tables

Figures

◀

▶

◀

▶

Back

Close

Full Screen / Esc

Printer-friendly Version

Interactive Discussion



this generally degrades the agreement with the independent observations, especially the ozonesonde observations made in the lower and middle troposphere. Introducing an adaptive localization technique that considers the structures of the chemical lifetime and atmospheric circulation, or increasing the ensemble size may be useful to improve the efficiency with which remote observations are used.

### 6.1.4 Total systematic error

The total error on the estimate of the LNO<sub>x</sub> source will be dominated by systematic errors such as the ones discussed above. The uncertainty caused by the ensemble spread was found to be small compared to the numbers given in Table 5. From the systematic satellite and model uncertainties listed in Table 5 we obtain an error estimate of about 1 TgNyr<sup>-1</sup> (0.7 in January, 1.6 in July), if we assume that the individual systematic error sources are uncorrelated. Apart from these sensitivity experiments (summarised in Table 5) several other sources of error may be introduced. In particular, Stavrakou et al. (2013) claimed that the uncertainty in the loss processes is very large for NO<sub>x</sub> resulting in a factor of 1.8 difference between upper and lower estimates of the LNO<sub>x</sub> source. This would translate into an error bar of about 1 TgNyr<sup>-1</sup>. If such an effect is added to the results in Table 5, the total error bar would increase to about 1.4 TgNyr<sup>-1</sup>.

## 6.2 Implication for the parameterization of LNO<sub>x</sub>

### 6.2.1 Flash activity

With respect to the climatology based on satellite observations, the scheme of Price and Rind (1992) overestimated the flash activity over South America but underestimated that over central Africa and over most of the tropical convergence zones, as reported in previous studies (e.g. Allen and Pickering, 2002; Labrador et al., 2005; Martin et al., 2007). The modelling of the flash rate may be improved by using a more

advanced parameterisation. However, Tost et al. (2007) concluded that the observed lightning distributions were not even approximately reproduced with any of the lightning parameterisations based on either cloud-top height, updraft velocity, updraft mass flux, or convective precipitation.

Murray et al. (2012) demonstrated that applying monthly scaling factors obtained from the LIS/OTD satellite instruments improves the tropical ozone simulation. However, we found that the simulated concentrations are only slightly changed by scaling the global lightning flash count to the climatological observations from the LIS/OTD. The observations cannot be used to adjust the detailed spatial structure of the flash frequency because of the small amount of coverage on a daily basis. On the other hand, an increase in the annual LNO<sub>x</sub> amount from 4.7 to 6.3 TgNyr<sup>-1</sup> is obtained from assimilation but cannot simply be explained by a roughly 7% underestimation of the global lightning flash frequency as compared to the LIS/OTD climatology. Various factors, such as for instance the NO<sub>x</sub> production per flash, are responsible for uncertainty in the LNO<sub>x</sub> source parameterisation. Meanwhile, the relative positive adjustment of the lightning source is larger over the oceans compared to land (58% vs. 30%). This finding may indicate that the power 1.73 in the modelling of the height dependence of the lightning activity over ocean is underestimated in the Price and Rind (1992) approach.

## 6.2.2 NO<sub>x</sub> production per flash and CG/IC ratio

Even if the flash frequency could be predicted accurately by the model, an uncertainty in the amount of NO<sub>x</sub> produced per flash would lead to an error in the LNO<sub>x</sub> source estimates. The annual global LNO<sub>x</sub> source from our estimates corresponds to a mean NO production of about 350 mol flash<sup>-1</sup>. This value is within the range of most other recent estimates. For instance, Schumann and Huntrieser (2007) suggested a best estimate of 250 mol NO flash<sup>-1</sup>. Ott et al. (2010) reported a mean value of 500 mol flash<sup>-1</sup> from a cloud-resolved modelling analysis of mid-latitude and sub-tropical storms. Hudman et al. (2007) and Jourdain et al. (2010) showed, respectively, that a continental pro-

## Lightning NO<sub>x</sub> production estimation

K. Miyazaki et al.

Title Page

Abstract

Introduction

Conclusions

References

Tables

Figures

◀

▶

◀

▶

Back

Close

Full Screen / Esc

Printer-friendly Version

Interactive Discussion



Lightning NO<sub>x</sub>  
production  
estimation

K. Miyazaki et al.

Title Page

Abstract

Introduction

Conclusions

References

Tables

Figures

◀

▶

◀

▶

Back

Close

Full Screen / Esc

Printer-friendly Version

Interactive Discussion



duction rate of 500 or 520 mol NO flash<sup>-1</sup> gives reasonable performance in a chemical simulation over the United States. Boersma et al. (2005) used the Global Ozone Monitoring Experiment (GOME) NO<sub>2</sub> data and estimated a global LNO<sub>x</sub> source strength of 1.6–6.4 Tg N yr<sup>-1</sup>, implying a production rate of 82–328 mol NO flash<sup>-1</sup> based on the LIS/OTD climatology.

The amount of NO<sub>x</sub> produced per flash may not be constant over the globe. It varies with flash strength, extension, type, branching, and other factors. Huntrieser et al. (2008) suggested that tropical thunderstorms are less effective than mid-latitude storms in LNO<sub>x</sub> production per flash due to lower wind shears and smaller stroke lengths. Our analysis for July consistently reveals a large production per flash of 430 mol of NO in the NH (20–90° N) compared to 360 mol of NO in the tropics (20° S–20° N) based on the parameterised flash rate. Detailed analyses of individual storms with a high-resolution model are required to provide insights into the NO production efficiency for individual cases.

A large uncertainty also remains regarding the ratio of NO<sub>x</sub> production per flash by IC and CG flashes. Following Price et al. (1997), a lightning NO production of 1100 mol (CG flash)<sup>-1</sup> and 110 mol (IC flash)<sup>-1</sup> was assumed in the parameterisation. However, it has been suggested that the ratio should be closer to 1 than to 10 (Gallardo and Cooray, 1996; Fehr et al., 2004; DeCaria et al., 2005). We attempted to optimize these parameters from the multi-species data assimilation but could not find any significant differences between the two parameters in the analysis. The observational constraints still seem insufficient for optimizing such detailed parameters. Further insights may be obtained with observations that are higher in accuracy, density, and vertical resolution.

### 6.2.3 The C-shaped vertical profile

The assumption of a C-shaped vertical profile as proposed by Pickering et al. (1998) implies that a majority of the LNO<sub>x</sub> is present in the upper troposphere, while a secondary

## Lightning NO<sub>x</sub> production estimation

K. Miyazaki et al.

Title Page

Abstract

Introduction

Conclusions

References

Tables

Figures

◀

▶

◀

▶

Back

Close

Full Screen / Esc

Printer-friendly Version

Interactive Discussion



maximum occurs in the boundary layer as a result of downdrafts. Our data assimilation analysis suggests that the C-shape assumption underestimates the source strength in the middle and upper troposphere over land. Ott et al. (2010) reported a consistent result from analyses of a cloud-scale chemical transport model. They also suggested that the upper tropospheric maximum in LNO<sub>x</sub> mass may be located too high because of the C-shape assumption at mid-latitudes. Our analysis also revealed that the peak source height is overestimated by up to about 1 km in the tropics. Ott et al. (2010) suggested that the simplified treatment of LNO<sub>x</sub> and wind fields by Pickering et al. (1998) will cause errors in the vertical LNO<sub>x</sub> source profile.

The robustness of the analysed vertical profile of the LNO<sub>x</sub> source in the assimilation was evaluated with an assimilation sensitivity experiment that optimized height-independent source scaling factors for each grid point. Compared to the height-independent analysis, the height-dependent analysis (i.e. the standard data assimilation) produces sources larger by 24 % at 300 hPa in January, and sources smaller by 14 % at 200 hPa in July in the tropics (20° S–20° N) for grid points with the LNO<sub>x</sub> source column greater than  $5 \times 10^{-15} \text{ kg m}^{-2} \text{ s}^{-1}$  (figure not shown). In both seasons, the height-dependent analysis generally produces a lower peak height for the source in the upper troposphere. The global sources also exhibit systematic differences between the assimilations with height-independent and height-dependent source factors (Table 3). The two estimations show a large discrepancy especially when TES O<sub>3</sub> data are assimilated. In the height-dependent analysis, it was estimated that the TES data assimilation mostly decreases the LNO<sub>x</sub> sources in the upper troposphere (c.f., Fig. 8). In contrast, in the height-independent analysis, the LNO<sub>x</sub> sources are increased throughout the troposphere, because positive increments obtained by the constraints in the middle troposphere mostly dominate the total adjustment. These results demonstrate the capability of the simultaneous assimilation of multiple datasets to modify the vertical source shape.

### 6.3 Validation using forward CTM simulations

The O<sub>3</sub> concentrations simulated using the estimated lightning and surface sources in CHASER are used to indirectly validate the performance of the estimated sources, as summarized in Table 6. In the validation, the multiplication factors for the LNO<sub>x</sub> sources and the surface emissions estimated from the assimilation are used as inputs to forward CHASER simulations without adjusting the chemical concentrations by assimilation. The validation is made when lightning is active; e.g. for July in the NH and for January in the tropics and the SH. The ozonesonde observations from 39 locations were taken from the World Ozone and Ultraviolet Data Center (WOUDC)/Southern Hemisphere Additional Ozonesondes (SHADOZ) database, as in Miyazaki et al. (2012a). By using the estimated LNO<sub>x</sub> sources instead of the sources predicted by the model parameterization, CHASER simulations showed improved agreement with independent global ozonesonde observations. The improved agreement includes 13 % reductions in the negative bias in the middle/upper troposphere for the NH, 17 % reductions in the positive bias in the upper troposphere for the tropics, and about 25–50 % reductions in the positive bias in the middle/upper troposphere for the SH. The CHASER simulation showed further improved agreement with the ozonesonde observations, by using the surface NO<sub>x</sub> emission data from the multiple data assimilation instead of the emission inventories, together with the estimated LNO<sub>x</sub> sources. This reduced the ozone bias in the NH and the tropics throughout the troposphere. These results demonstrate the improved consistency of the concentrations and emissions through the multiple datasets assimilation and confirm the quality of the estimated sources as inputs to CTM simulations. We note that the concentration adjustment by the simultaneous data assimilation play an important role in further improving the ozone fields especially in the upper troposphere and the lower stratosphere.

## 6.4 Comparisons with previous estimates

Based on various estimation results, Schumann and Huntrieser (2007) have provided a best estimate of  $5 \pm 3 \text{ Tg Nyr}^{-1}$  for the annual global  $\text{LNO}_x$  source. Our estimate of  $6.3 \pm 1.4 \text{ Tg Nyr}^{-1}$  is well within the range of the best estimate. This is small compared to recent estimates of the uncertainty in the lightning sources (Schumann and Huntrieser, 2007). More recently, Murray et al. (2012) and Stavrou et al. (2013) estimated a global annual  $\text{LNO}_x$  source of  $6 \pm 0.5 \text{ Tg Nyr}^{-1}$  and  $3.3\text{--}5.9 \text{ Tg Nyr}^{-1}$ , respectively. These estimates are also close to our estimate. In spite of the good agreement in the estimates of the annual global source, the  $\text{LNO}_x$  source varies significantly with season and year, and differences will be more pronounced when comparisons are made regionally. Detailed comparisons on monthly and regional scales including those seasonal variations remain an important topic for future studies.

## 7 Conclusions

The global source of lightning-produced  $\text{NO}_x$  ( $\text{LNO}_x$ ) is estimated from an assimilation of multiple chemical species based on an ensemble Kalman filter approach.  $\text{NO}_2$ ,  $\text{O}_3$ ,  $\text{HNO}_3$ , and CO measurements obtained from multiple satellite instruments (OMI, MLS, TES, and MOPITT) provide comprehensive constraints on estimates of the global  $\text{LNO}_x$  source. This approach has the potential to reduce the influence of model errors on the  $\text{LNO}_x$  source estimation by simultaneously optimizing various aspects of the chemical system, including the surface emissions of  $\text{NO}_x$  and CO as well as the concentrations of 35 chemical species. Errors in these model fields other than the  $\text{LNO}_x$  sources introduce additional model–observation mismatches into the inversion and degrade the  $\text{LNO}_x$  source estimation. In most previous top-down estimates, only  $\text{LNO}_x$  sources were optimized from  $\text{NO}_2$  measurements. In such cases, the  $\text{LNO}_x$  sources may be overcorrected since analysis increments are introduced to compensate for various sources of model error. Substantial differences in the estimated  $\text{LNO}_x$  sources are

### Lightning $\text{NO}_x$ production estimation

K. Miyazaki et al.

Title Page

Abstract

Introduction

Conclusions

References

Tables

Figures

◀

▶

◀

▶

Back

Close

Full Screen / Esc

Printer-friendly Version

Interactive Discussion



obtained between the single-parameter ( $\text{LNO}_x$ ) inversion and the combined optimization of sources and concentrations, which emphasizes the ability of the assimilation system presented in this paper to improve the  $\text{LNO}_x$  source estimation.

The assimilation provides substantial adjustments to the  $\text{NO}_x$  sources both at the surface and in the middle–upper troposphere, because of the use of multiple satellite data sets with different vertical sensitivities, see Fig. 1. The relative importance of the individual assimilated datasets varies with height and season, reflecting the measurement sensitivity and its relation to lightning activity. The cloud-covered OMI  $\text{NO}_2$  retrievals provide important constraints on the estimation of the  $\text{LNO}_x$  above, and inside the upper part of clouds, because of the enhanced measurement sensitivity of air masses transported upward by the deep convection. TES and MLS measurements add important constraints on the vertical profiles of the  $\text{LNO}_x$  sources, especially in the upper troposphere. Regional studies of the atmosphere over Africa and the western Pacific demonstrated that the optimization of multiple chemical aspects is a powerful approach for correcting various processes controlling variations in  $\text{O}_3$  and  $\text{NO}_2$ .

The annual global  $\text{LNO}_x$  source amount and  $\text{NO}$  production efficiency for 2007 are estimated by the assimilation system to be  $6.3 \text{ Tg N yr}^{-1}$  and  $350 \text{ mol NO flash}^{-1}$ , respectively, which are within the ranges of recent values from top-down estimations and cloud-resolving simulations. The total error on the mean global  $\text{LNO}_x$  source due to uncertainties in the observation, the model, and the assimilation settings have been studied with a series of sensitivity experiments and is estimated as  $1.4 \text{ Tg N yr}^{-1}$ .

The annual  $\text{LNO}_x$  source columns are increased over most parts of the land by up to about 40 % compared to the a priori emissions predicted using the  $\text{LNO}_x$  parameterization. The analyzed  $\text{LNO}_x$  sources exhibit obvious regional differences in the tropics, reflecting the regionality of cumulus convection and monsoon circulation. The analysis increments significantly differ between land and the oceans, with annual global source increases of about 56 % over the oceans and by about 32 % over land. These increases are largely attributed to the positive increments in the lower troposphere over the oceans and in the upper troposphere over land. We find that the relative pos-

## Lightning $\text{NO}_x$ production estimation

K. Miyazaki et al.

Title Page

Abstract

Introduction

Conclusions

References

Tables

Figures

◀

▶

◀

▶

Back

Close

Full Screen / Esc

Printer-friendly Version

Interactive Discussion



## Lightning NO<sub>x</sub> production estimation

K. Miyazaki et al.

Title Page

Abstract

Introduction

Conclusions

References

Tables

Figures

◀

▶

◀

▶

Back

Close

Full Screen / Esc

Printer-friendly Version

Interactive Discussion



itive adjustment of the lightning source is significantly larger over the oceans compared to land. This finding may indicate that the power 1.73 in the modelling of the height dependence of the source over ocean is underestimated. The significantly improved agreement with independent ozone observations from ozonesondes and TOC retrievals gives confidence in the performance of the data assimilation.

The analysed LNO<sub>x</sub> sources have important implications for improving LNO<sub>x</sub> parameterisations. First, errors in flash rates can explain only a small fraction of the uncertainty in LNO<sub>x</sub> estimates. The remaining uncertainty in estimates from the bottom-up approach arises from the NO production efficiency that can be very different for individual storms. Our analysis suggests that tropical thunderstorms are less effective than mid-latitude storms in generating NO with each flash, as commonly suggested by previous studies. Second, the widely used C-shape assumption underestimates the source strength in the upper troposphere and overestimates the peak source height over land and the tropical oceans, especially along the ITCZ. Finally, as the two types of discharges (IC and CG) behave differently, these should be considered separately. Although parameters related to these different types are hardly discriminated with the currently available observations, the approach of combining all available satellite datasets is expected to provide further insights into such detailed processes in future studies with measurements that are more advanced (i.e. higher in accuracy, density, and vertical resolution).

*Acknowledgements.* We would like to thank Masayuki Takigawa, Hisashi Yashiro, Kevin Hamilton, Yuqing Wang, and Folkert Boersma for their helpful comments on this study. This work was supported by the JSPS Grant-in-Aid for Young Scientists (B) 24740327.

## References

Allen, D. J. and Pickering, K. E.: Evaluation of lightning flash rate parameterizations for use in a global chemical transport model, *J. Geophys. Res.*, 107, 4711, doi:10.1029/2002JD002066, 2002.

## Lightning NO<sub>x</sub> production estimation

K. Miyazaki et al.

Title Page

Abstract

Introduction

Conclusions

References

Tables

Figures

◀

▶

◀

▶

Back

Close

Full Screen / Esc

Printer-friendly Version

Interactive Discussion



- Arakawa, A. and Schubert, W. H.: The interaction of a cumulus cloud ensemble with the large-scale environment, *J. Atmos. Sci.*, 31, 674–701, 1974.
- Beirle, S., Spichtinger, N., Stohl, A., Cummins, K. L., Turner, T., Boccippio, D., Cooper, O. R., Wenig, M., Grzegorski, M., Platt, U., and Wagner, T.: Estimating the NO<sub>x</sub> produced by lightning from GOME and NLDN data: a case study in the Gulf of Mexico, *Atmos. Chem. Phys.*, 6, 1075–1089, doi:10.5194/acp-6-1075-2006, 2006.
- Boccippio, D. J.: Lightning scaling relations revisited, *J. Atmos. Sci.*, 59, 1086–1104, 2002.
- Boersma, K. F., Eskes, H. J., Meijer, E. W., and Kelder, H. M.: Estimates of lightning NO<sub>x</sub> production from GOME satellite observations, *Atmos. Chem. Phys.*, 5, 2311–2331, doi:10.5194/acp-5-2311-2005, 2005.
- Boersma, K. F., Eskes, H. J., Dirksen, R. J., van der A, R. J., Veefkind, J. P., Stammes, P., Huijnen, V., Kleipool, Q. L., Sneep, M., Claas, J., Leitão, J., Richter, A., Zhou, Y., and Brunner, D.: An improved tropospheric NO<sub>2</sub> column retrieval algorithm for the Ozone Monitoring Instrument, *Atmos. Meas. Tech.*, 4, 1905–1928, doi:10.5194/amt-4-1905-2011, 2011.
- Bowman, K. W., Rodgers, C. D., Sund-Kulawik, S., Worden, J., Sarkissian, E., Osterman, G., Steck, T., Luo, M., Eldering, A., Shephard, M. W., Worden, H., Clough, S. A., Brown, P. D., Rinsland, C. P., Lampel, M., Gunson, M., and Beer, R.: Tropospheric emission spectrometer: retrieval method and error analysis, *IEEE T. Geosci. Remote*, 44, 1297–1307, 2006.
- Cooper, O. R., Stohl, A., Trainer, M., Thompson, A. M., Witte, J. C., Oltmans, S., Morris, G. A., Pickering, K. E., Crawford, J., Chen, G., Cohen, R. C., Bertram, T. H., Wooldridge, P. J., Perrington, A., Brune, W. H., Merrill, J., Moody, J., Tarasick, D., Nédélec, P., Forbes, G., Newchurch, M., Schmidlin, F., Johnson, B. J., Turquety, S., Baughcum, S. L., Ren, X., Fehsenfeld, F., Meagher, J. F., Spichtinger, N., Brown, C., McKeen, S. A., McDermid, I., and Leblanc, T.: Large upper tropospheric ozone enhancements above mid-latitude North America during summer: in situ evidence from the IONS and MOZAIC ozone measurement network, *J. Geophys. Res.*, 111, D24S05, doi:10.1029/2006JD007306, 2006.
- Christian, H. J., Blakeslee, R. J., Boccippio, D. J., Boeck, W. L., Buechler, D. E., Driscoll, K. T., Goodman, S. J., Hall, J. M., Koshak, W. J., Mach, D. M., and Stewart, M. F.: Global frequency and distribution of lightning as observed from space by the Optical Transient Detector, *J. Geophys. Res.*, 108, 4005, doi:10.1029/2002JD002347, 2003.
- DeCaria, A. J., Pickering, K. E., Stenchikov, G. L., Scala, J. R., Stith, J. L., Dye, J. E., Ridley, B. A., and Laroche, P.: A cloud-scale model study of lightning-generated NO<sub>x</sub> in an individual thunderstorm during STERAO-A, *J. Geophys. Res.*, 105, 11601–11616, 2000.

Lightning NO<sub>x</sub>  
production  
estimation

K. Miyazaki et al.

Title Page

Abstract

Introduction

Conclusions

References

Tables

Figures

◀

▶

◀

▶

Back

Close

Full Screen / Esc

Printer-friendly Version

Interactive Discussion



- DeCaria, A. J., Pickering, K. E., Stenchikov, G. L., and Ott, L. E.: Lightning-generated NO<sub>x</sub> and its impact on tropospheric ozone production: a three-dimensional modeling study of a Stratosphere-Troposphere Experiment: Radiation, Aerosols and Ozone (STERAO-A) thunderstorm, *J. Geophys. Res.*, 110, 1–13, doi:10.1029/2004JD005556, 2005.
- 5 Deeter, M. N., Martinez-Alonso, S., Edwards, D. P., Emmons, L. K., Gille, J. C., Worden, H. M., Pittman, J. V., Daube, B. C., and Wofsy, S. C.: Validation of MOPITT Version 5 thermal-infrared, near-infrared, and multispectral carbon monoxide profile retrievals for 2000–2011, *J. Geophys. Res. Atmos.*, 118, 6710–6725, doi:10.1002/jgrd.50272, 2003.
- 10 Deeter, M. N., Worden, H. M., Edwards, D. P., Gille, J. C., Mao, D., and Drummond, J. R.: MOPITT multispectral CO retrievals: origins and effects of geophysical radiance errors, *J. Geophys. Res.*, 116, D15303, doi:10.1029/2011JD015703, 2011.
- Deeter, M. N., Martinez-Alonso, S., Edwards, D. P., Emmons, L. K., Gille, J. C., Worden, H. M., Pittman, J. V., Daube, B. C., and Wofsy, S. C.: Validation of MOPITT Version 5 thermal-infrared, near-infrared, and multispectral carbon monoxide profile retrievals for 2000–2011, *J. Geophys. Res. Atmos.*, 118, 6710–6725, doi:10.1002/jgrd.50272, 2013.
- 15 Emori, S., Hasegawa, A., Suzuki, T., and Dairaku, K.: Validation, parameterization dependence, and future projection of daily precipitation simulated with a high-resolution atmospheric GCM, *Geophys. Res. Lett.*, 32, L06708, doi:10.1029/2004GL022306, 2005.
- Fehr, T., Höller, H., and Huntrieser, H.: Model study on production and transport of lightning-produced NO<sub>x</sub> in a EULINOX supercell storm, *J. Geophys. Res.*, 109, 1–17, doi:10.1029/2003JD003935, 2004.
- 20 Gallardo, L. and Cooray, V.: Could cloud-to-cloud discharges be as effective as cloud-to-ground discharges in producing NO<sub>x</sub>?, *Tellus B*, 48, 641–651, 1996.
- Gaspari, G. and Cohn, S. E.: Construction of correlation functions in two and three dimensions, *Q. J. Roy. Meteor. Soc.*, 125, 723–757, 1999.
- 25 Graedel, T. E., Bates, T. S., Bouwman, A. F., Cunnold, D., Dignon, J., Fung, I., Jacob, D. J., Lamb, B. K., Logan, J. A., Marland, G., Middleton, P., Pacyna, J. M., Placet, M., and Veldt, C.: A compilation of inventories of emissions to the atmosphere, *Global Biogeochem. Cy.*, 7, 1–26, 1993.
- 30 Hudman, R. C., Jacob, D. J., Turquety, S., Leibensperger, E. M., Murray, L. T., Wu, S., Gilliland, A. B., Avery, M., Bertram, T. H., Brune, W., Cohen, R. C., Dibb, J. E., Flocke, F. M., Fried, A., Holloway, J., Neuman, J. A., Orville, R., Perring, A., Ren, X., Ryerson, T. B., Sachse, G. W., Singh, H. B., Swanson, A., and Wooldridge, P. J.: Surface and lightning sources of nitrogen

Lightning NO<sub>x</sub>  
production  
estimation

K. Miyazaki et al.

Title Page

Abstract

Introduction

Conclusions

References

Tables

Figures

◀

▶

◀

▶

Back

Close

Full Screen / Esc

Printer-friendly Version

Interactive Discussion

oxides over the United States: magnitudes, chemical evolution, and outflow, *J. Geophys. Res.*, 112, D12S05, doi:10.1029/2006JD007912, 2007.

Hunt, B. R., Kostelich, E. J., and Szunyogh, I.: Efficient data assimilation for spatiotemporal chaos: a local ensemble transform Kalman filter, *Physica D*, 230, 112–126, 2007.

Huntrieser, H., Schumann, U., Schlager, H., Höller, H., Giez, A., Betz, H.-D., Brunner, D., Forster, C., Pinto Jr., O., and Calheiros, R.: Lightning activity in Brazilian thunderstorms during TROCCINOX: implications for NO<sub>x</sub> production, *Atmos. Chem. Phys.*, 8, 921–953, doi:10.5194/acp-8-921-2008, 2008.

Jenkins, G. S. and Ryu, J.-H.: Space-borne observations link the tropical atlantic ozone maximum and paradox to lightning, *Atmos. Chem. Phys.*, 4, 361–375, doi:10.5194/acp-4-361-2004, 2004.

Jourdain, L., Worden, H. M., Worden, J. R., Bowman, K., Li, Q. B., Eldering, A., Kulawik, S. S., Osterman, G., Boersma, F., Fisher, B., Rinsland, C. P., Beer, R., and Gunson, M.: Tropospheric vertical distribution of tropical Atlantic ozone observed by TES during the Northern African biomass burning season, *Geophys. Res. Lett.*, 34, L04810, doi:10.1029/2006GL028284, 2007.

Jourdain, L., Kulawik, S. S., Worden, H. M., Pickering, K. E., Worden, J., and Thompson, A. M.: Lightning NO<sub>x</sub> emissions over the USA constrained by TES ozone observations and the GEOS-Chem model, *Atmos. Chem. Phys.*, 10, 107–119, doi:10.5194/acp-10-107-2010, 2010.

Kanamitsu, M., Ebisuzaki, W., Woollen, J., Yang, S. K., Hnilo, J. J., Fiorino, M., and Potter, G. L.: NCEP-DOE AMIP-II reanalysis (R-2), *B. Am. Meteorol. Soc.*, 83, 1631–1643, doi:10.1175/BAMS-83-11-1631, 2002.

Labrador, L. J., von Kuhlmann, R., and Lawrence, M. G.: The effects of lightning-produced NO<sub>x</sub> and its vertical distribution on atmospheric chemistry: sensitivity simulations with MATCH-MPIC, *Atmos. Chem. Phys.*, 5, 1815–1834, doi:10.5194/acp-5-1815-2005, 2005.

Lay, E. H., Jacobson, A. R., Holzworth, R. H., Rodger, C. J., and Dowden, R. L.: Local time variation in land/ocean lightning flash density as measured by the World Wide Lightning Location Network, *J. Geophys. Res.*, 112, D13111, doi:10.1029/2006JD007944, 2007.

Lin, J.-T.: Satellite constraint for emissions of nitrogen oxides from anthropogenic, lightning and soil sources over East China on a high-resolution grid, *Atmos. Chem. Phys.*, 12, 2881–2898, doi:10.5194/acp-12-2881-2012, 2012.

**Lightning NO<sub>x</sub>  
production  
estimation**

K. Miyazaki et al.

Title Page

Abstract

Introduction

Conclusions

References

Tables

Figures

◀

▶

◀

▶

Back

Close

Full Screen / Esc

Printer-friendly Version

Interactive Discussion

- Livesey, N. J., Read, W. G., Froidevaux, L., Lambert, A., Manney, G. L., Pumphrey, H. C., Santee, M. L., Schwartz, M. J., Wang, S., Cofield, R. E., Cuddy, D. T., Fuller, R. A., Jarnot, R. F., Jiang, J. H., Knosp, B. W., Stek, P. C., Wagner, P. A., and Wu, D. L.: Aura Microwave Limb Sounder (MLS), Version 3.3 Level 2 data quality and description document, Tech. Rep. JPL D-33509, Jet Propul. Lab., Pasadena, CA, 2011.
- Martin, R. V., Jacob, D. J., Logan, J. A., Ziemke, J. M., and Washington, R.: Detection of a lightning influence on tropical tropospheric ozone, *Geophys. Res. Lett.*, 27, 1639–1642, 2000.
- Martin, R. V., Sauvage, B., Folkens, I., Sioris, C. E., Boone, C., Bernath, P., and Ziemke, J. R.: Space-based constraints on the production of nitric oxide by lightning, *J. Geophys. Res.*, 112, D09309, doi:10.1029/2006JD007831, 2007.
- Ménard, R. and Chang, L.-P.: Assimilation of stratospheric chemical tracer observations using a Kalman filter, Part 2: 2-validated results and analysis of variance and correlation dynamics, *Mon. Weather Rev.*, 128, 2672–2686, 2000.
- Miyazaki, K. and Eskes, H.: Constraints on surface NO<sub>x</sub> emissions by assimilating satellite observations of multiple species, *Geophys. Res. Lett.*, 40, 4745–4750, doi:10.1002/grl.50894, 2013.
- Miyazaki, K., Eskes, H. J., Sudo, K., Takigawa, M., van Weele, M., and Boersma, K. F.: Simultaneous assimilation of satellite NO<sub>2</sub>, O<sub>3</sub>, CO, and HNO<sub>3</sub> data for the analysis of tropospheric chemical composition and emissions, *Atmos. Chem. Phys.*, 12, 9545–9579, doi:10.5194/acp-12-9545-2012, 2012a.
- Miyazaki, K., Eskes, H. J., and Sudo, K.: Global NO<sub>x</sub> emission estimates derived from an assimilation of OMI tropospheric NO<sub>2</sub> columns, *Atmos. Chem. Phys.*, 12, 2263–2288, doi:10.5194/acp-12-2263-2012, 2012b.
- Murray, L. T., Jacob, D. J., Logan, J. A., Hudman, R. C., and Koshak, W. J.: Optimized regional and interannual variability of lightning in a global chemical transport model constrained by LIS/OTD satellite data, *J. Geophys. Res.*, 117, D20307, doi:10.1029/2012JD017934, 2012.
- Nassar, R., Logan, J. A., Worden, H. M., Megretskaia, I. A., Bowman, K. W., Osterman, G. B., Thompson, A. M., Tara-sick, D. W., Austin, S., Claude, H., Dubey, M. K., Hocking, W. K., Johnson, B. J., Joseph, E., Merrill, J., Morris, G. A., Newchurch, M., Oltmans, S. J., Posny, F., Schmidlin, F. J., Vomel, H., Whiteman, D. N., and Witte, J. C.: Validation of Tropospheric Emission Spectrometer (TES) nadir ozone profiles using ozonesonde measurements, *J. Geophys. Res.*, 113, D15S17, doi:10.1029/2007JD008819, 2008.

**Lightning NO<sub>x</sub>  
production  
estimation**

K. Miyazaki et al.

Title Page

Abstract

Introduction

Conclusions

References

Tables

Figures

◀

▶

◀

▶

Back

Close

Full Screen / Esc

Printer-friendly Version

Interactive Discussion



- Ott, L. E., Pickering, K. E., Stenchikov, G. L., Allen, D. J., DeCaria, A. J., Ridley, B., Lin, R.-F., Lang, S., and Tao, W.-K.: Production of lightning NO<sub>x</sub> and its vertical distribution calculated from three-dimensional cloud-scale chemical transport model simulations, *J. Geophys. Res.*, 115, D04301, doi:10.1029/2009JD011880, 2010.
- 5 Pan, D.-M., and Randall, D. A.: A cumulus parameterization with a prognostic closure, *Q. J. Roy. Meteor. Soc.*, 124, 949–981, 1998.
- Pickering, K. E., Wang, Y., Tao, W. K., Price, C., and Muller, J. F.: Vertical distributions of lightning NO<sub>x</sub> for use in regional and global chemical transport models, *J. Geophys. Res.*, 103, 31203–31216, doi:10.1029/98JD02651, 1998.
- 10 Price, C. and Rind, D.: A simple lightning parameterization for calculating global lightning distributions, *J. Geophys. Res.*, 97, 9919–9933, doi:10.1029/92JD00719, 1992.
- Price, C., Penner, J., and Prather, M.: NO<sub>x</sub> from lightning, 1. Global distribution based on lightning physics, *J. Geophys. Res.*, 102, 5929–5941, doi:10.1029/96JD03504, 1997.
- Ridley, B. A., Dye, J. E., Walega, J. G., Zheng, J., Grahek, F. E., and Rison, W.: On the production of active nitrogen by thunderstorms over New Mexico, *J. Geophys. Res.*, 101, 20985–21005, doi:10.1029/96JD01706, 1996.
- 15 Schumann, U. and Huntrieser, H.: The global lightning-induced nitrogen oxides source, *Atmos. Chem. Phys.*, 7, 3823–3907, doi:10.5194/acp-7-3823-2007, 2007.
- Skamarock, W. C., Klemp, J. B., Dudhia, J., Gill, D. O., Barker, D. M., Wang, W., and Powers, J. G.: A description of the Advanced Research WRF Version 3, NCAR Tech Notes-475+STR, 113 pp., 2008.
- 20 Stavrou, T., Müller, J.-F., Boersma, K. F., van der A, R. J., Kurokawa, J., Ohara, T., and Zhang, Q.: Key chemical NO<sub>x</sub> sink uncertainties and how they influence top-down emissions of nitrogen oxides, *Atmos. Chem. Phys.*, 13, 9057–9082, doi:10.5194/acp-13-9057-2013, 2013.
- 25 Sudo, K., Takahashi, M., and Akimoto, H.: CHASER: a global chemical model of the troposphere, 2. Model results and evaluation, *J. Geophys. Res.*, 107, 4586, doi:10.1029/2001JD001114, 2002.
- Thompson, A. M., Pickering, K. E., Dickerson, R. R., Ellis Jr., W. G., Jacob, D. J., Scala, J. R., Tao, W.-K., McNamara, D. P., and Simpson, J.: Convective transport over the central United States and its role in regional CO and ozone budgets, *J. Geophys. Res.*, 99, 18703–18711, doi:10.1029/94JD01244, 1994.
- 30

**Lightning NO<sub>x</sub>  
production  
estimation**

K. Miyazaki et al.

Title Page

Abstract

Introduction

Conclusions

References

Tables

Figures

◀

▶

◀

▶

Back

Close

Full Screen / Esc

Printer-friendly Version

Interactive Discussion



Thompson, A. M., Witte, J. C., Smit, H. G. J., Oltmans, S. J., Johnson, B. J., Kirchhoff, V. W. J. H., and Schmidlin, F. J.: Southern Hemisphere Additional Ozonesondes (SHADOZ) 1998–2004 tropical ozone climatology: 3. Instrumentation, station-to-station variability, and evaluation with simulated flight profiles, *J. Geophys. Res.*, 112, D03304, doi:10.1029/2005JD007042, 2007.

Tost, H., Jöckel, P., and Lelieveld, J.: Lightning and convection parameterisations – uncertainties in global modelling, *Atmos. Chem. Phys.*, 7, 4553–4568, doi:10.5194/acp-7-4553-2007, 2007.

van der Werf, G. R., Randerson, J. T., Giglio, L., Collatz, G. J., Mu, M., Kasibhatla, P. S., Morton, D. C., DeFries, R. S., Jin, Y., and van Leeuwen, T. T.: Global fire emissions and the contribution of deforestation, savanna, forest, agricultural, and peat fires (1997–2009), *Atmos. Chem. Phys.*, 10, 11707–11735, doi:10.5194/acp-10-11707-2010, 2010.

Worden, J., Kulawik, S. S., Shephard, M. W., Clough, S. A., Worden, H., Bowman, K., and Goldman, A.: Predicted errors of tropospheric emission spectrometer nadir retrievals from spectral window selection, *J. Geophys. Res.*, 109, D09308, doi:10.1029/2004JD004522, 2004.

Worden, J., Liu, X., Bowman, K., Chance, K., Beer, R., Eldering, A., Gunson, M., and Worden, H.: Improved tropospheric ozone profile retrievals using OMI and TES radiances, *J. Geophys. Res.*, 34, L01809, doi:10.1029/2006GL027806, 2007.

Worden, J., Jones, D. B. A., Liu, J., Parrington, M., Bowman, K., Stajner, I., Beer, R., Jiang, J., Thouret, V., Kulawik, S., Li, J. L. F., Verma, S., and Worden, H.: Observed vertical distribution of tropospheric ozone during the Asian summertime monsoon, *J. Geophys. Res.*, 114, D13304, doi:10.1029/2008JD010560, 2009.

Ziemke, J. R., Chandra, S., Duncan, B. N., Froidevaux, L., Bhartia, P. K., Levelt, P. F., and Waters, J. W.: Tropospheric ozone determined from Aura OMI and MLS: evaluation of measurements and comparison with the Global Modeling Initiative's Chemical Transport Model, *J. Geophys. Res.*, 111, D19303, doi:10.1029/2006JD007089, 2006.

**Lightning NO<sub>x</sub>  
production  
estimation**

K. Miyazaki et al.

Title Page

Abstract

Introduction

Conclusions

References

Tables

Figures

◀

▶

◀

▶

Back

Close

Full Screen / Esc

Printer-friendly Version

Interactive Discussion



**Table 1.** The annual total LNO<sub>x</sub> sources (in TgNyr<sup>-1</sup>) obtained from the CTM simulation and the data assimilation for the Northern Hemisphere (NH, 20–90° N), the tropics (TR, 20° S–20° N), the Southern Hemisphere (SH, 90–20° S), and the globe (GL, 90° S–90° N). The analysis uncertainty estimated from the mean analysis spread is shown in brackets.

	NH	TR	SH	GL
CTM	1.4	2.7	0.6	4.7
Assimilation	2.0 (±0.3)	3.5 (±0.49)	0.8 (±0.10)	6.3 (±0.9)

## Lightning NO<sub>x</sub> production estimation

K. Miyazaki et al.

Title Page

Abstract

Introduction

Conclusions

References

Tables

Figures

◀

▶

◀

▶

Back

Close

Full Screen / Esc

Printer-friendly Version

Interactive Discussion



**Table 2.** The regional averages of the mean altitude (in km) with maximum annual LNO<sub>x</sub> emission (i.e., source peak height) estimated from the CTM simulation and the data assimilation. The analysis increments (the data assimilation minus the simulation) are shown in brackets. The definitions of the regions are same as for Fig. 6, except for the tropical western Pacific (130–165° E, 1–18° N). Grid points without any LNO<sub>x</sub> sources or with peak height for pressures higher than 850 hPa are removed from the average, in order to measure the upper tropospheric peak height.

	CTM	Assim	Increment
North America	7.82	7.85	+0.03
Europe	5.72	5.58	−0.14
Northern Eurasia	9.39	9.39	±0
Tropical Western Pacific	11.15	9.96	−1.19
South America	9.97	9.83	−0.14
Northern Africa	11.00	10.83	−0.17
Southern Africa	9.36	8.98	−0.38
Southeast Asia	11.51	10.77	−0.74
Australia	8.01	7.60	−0.41

Lightning NO<sub>x</sub>  
production  
estimation

K. Miyazaki et al.

**Table 3.** The monthly LNO<sub>x</sub> sources (in Tg N) for the Northern Hemisphere (NH, 20–90° N), the tropics (TR, 20° S–20° N), the Southern Hemisphere (SH, 90–20° S), and the globe (GL, 90° S–90° N) as obtained from the CTM simulation, the OSEs with TES O<sub>3</sub>, OMI NO<sub>2</sub>, MLS O<sub>3</sub>, and MLS HNO<sub>3</sub> observations, and from the assimilation of all the datasets. Also shown are results for data assimilation that optimizes a height-independent LNO<sub>x</sub> source scale factor (2-D). Standard deviations obtained from all the data assimilation estimates are also listed.

	Jan				Jul			
	NH	TR	SH	GL	NH	TR	SH	GL
CTM	0.58	2.82	0.95	4.35	3.17	2.41	0.31	5.89
TES O <sub>3</sub>	0.64	2.34	1.01	4.00	3.21	3.21	0.34	6.76
OMI NO <sub>2</sub>	0.78	3.25	1.20	5.22	3.99	3.51	0.51	8.01
MLS O <sub>3</sub>	0.74	4.89	1.21	6.84	4.82	4.69	0.31	9.83
MLS HNO <sub>3</sub>	0.82	4.89	1.89	7.56	4.33	3.66	0.31	8.30
ALL	0.78	3.99	1.39	6.15	4.69	2.99	0.50	8.18
TES O <sub>3</sub> (2-D)	0.72	3.35	1.67	5.75	4.94	3.74	0.37	9.05
OMI NO <sub>2</sub> (2-D)	0.78	3.29	1.12	5.18	2.86	3.54	0.49	6.89
MLS O <sub>3</sub> (2-D)	0.85	3.92	1.07	5.85	5.46	4.10	0.37	9.92
MLS HNO <sub>3</sub> (2-D)	0.74	3.66	1.34	5.75	3.93	2.80	0.33	7.07
ALL (2-D)	0.84	3.56	1.23	5.63	3.00	3.14	0.51	6.65
Standard dev.	0.07	0.77	0.28	0.96	0.89	0.56	0.09	1.23



Title Page

Abstract

Introduction

Conclusions

References

Tables

Figures

◀

▶

◀

▶

Back

Close

Full Screen / Esc

Printer-friendly Version

Interactive Discussion

Lightning NO<sub>x</sub>  
production  
estimation

K. Miyazaki et al.

[Title Page](#)[Abstract](#)[Introduction](#)[Conclusions](#)[References](#)[Tables](#)[Figures](#)[⏪](#)[⏩](#)[◀](#)[▶](#)[Back](#)[Close](#)[Full Screen / Esc](#)[Printer-friendly Version](#)[Interactive Discussion](#)

**Table 4.** The global spatial correlation (Corr), global mean difference (Bias), and global mean root-mean-square error (RMSE) of the three-monthly mean tropospheric O<sub>3</sub> columns (TOCs) for the OMI/MLS data of December–February (DJF) and June–August (JJA) in 2007. The results of the CTM simulation and data assimilation for 30° S–30° N are shown.

	DJF			JJA		
	Corr	Bias	RMSE	Corr	Bias	RMSE
CTM	0.85	1.92	4.16	0.92	1.41	3.26
Assim.	0.86	−0.55	2.85	0.92	0.19	2.59

Lightning NO<sub>x</sub>  
production  
estimation

K. Miyazaki et al.

**Table 5.** Similar to Table 3, but lists the LNO<sub>x</sub> sources obtained from the control data assimilation run (Control), with a 15 % addition of artificial OMI NO<sub>2</sub> bias (w/OMI bias), with the TES O<sub>3</sub> bias correction (TES bias corr.), without the OMI cloud-covered observations (w/o OMI cloud), with the SST data for 1997 (year 1997 SST), with 20 % increases in the convective mass flux (+20 % convection), with 20 % increases in the a priori errors of the LNO<sub>x</sub> source and the surface NO<sub>x</sub> emissions (+20 % LNO<sub>x</sub> err. and +20 % SNO<sub>x</sub> err.), and with 15 % increases in the a priori values of the LNO<sub>x</sub> sources (+15 % LNO<sub>x</sub> prior). The total bias due to all terms is computed as a random addition of the individual biases. See the text for details.

	Jan				Jul			
	NH	TR	SH	GL	NH	TR	SH	GL
Control	0.78	3.99	1.39	6.15	4.69	2.99	0.50	8.18
w/OMI bias	0.87	3.97	1.46	6.31	4.61	3.08	0.50	8.18
TES bias corr.	0.68	3.79	1.36	5.83	4.19	2.74	0.29	7.21
w/o cloud OMI	0.76	4.04	1.31	6.09	4.13	2.89	0.29	7.33
year 1997 SST	0.76	3.89	1.37	6.03	4.71	3.06	0.51	8.26
+20 % convection	0.80	3.76	1.37	5.89	4.27	2.99	0.50	8.09
+20 % LNO <sub>x</sub> err.	0.83	3.75	1.32	5.90	4.59	2.93	0.51	8.03
+20 % SNO <sub>x</sub> err.	0.81	3.77	1.27	5.85	4.58	2.83	0.50	7.90
+15 % LNO <sub>x</sub> prior	0.83	4.10	1.48	6.41	5.29	3.16	0.57	9.02
Total bias	0.16	0.47	0.20	0.66	1.06	0.38	0.31	1.58

Title Page

Abstract

Introduction

Conclusions

References

Tables

Figures

◀

▶

◀

▶

Back

Close

Full Screen / Esc

Printer-friendly Version

Interactive Discussion



Lightning NO<sub>x</sub>  
production  
estimation

K. Miyazaki et al.

**Table 6.** The mean ozone concentration bias (in ppbv) between the CHASER simulations and the global ozonesonde observations for January 2007 in the NH (25° N–90° N) and for July 2007 in the tropics (TR, 25° S–25° N) and the SH (90° S–25° S). The CHASER simulation results using the a priori emissions sources (A priori), the LNO<sub>x</sub> sources (LNO<sub>x</sub>), and the LNO<sub>x</sub> sources and surface NO<sub>x</sub> emissions (L + SNO<sub>x</sub>) are shown. The results from the CHASER-DAS simultaneous assimilation are also listed (DAS).

	NH in Jul				TR in Jan				SH in Jan			
	A priori	LNO <sub>x</sub>	L + SNO <sub>x</sub>	DAS	A priori	LNO <sub>x</sub>	L + SNO <sub>x</sub>	DAS	A priori	LNO <sub>x</sub>	L + SNO <sub>x</sub>	DAS
750–450 hPa	–12.3	–11.7	–0.2	–1.8	18.5	20.2	16.6	16.4	–4.1	–2.0	–2.8	–4.9
450–200 hPa	–6.8	–5.9	0.7	1.3	8.9	9.5	3.3	3.3	9.9	7.4	3.4	–1.0
200–90 hPa	19.8	19.7	4.8	4.5	42.2	34.9	21.7	10.4	219.5	136.2	149.5	45.3

Title Page

Abstract

Introduction

Conclusions

References

Tables

Figures

◀

▶

◀

▶

Back

Close

Full Screen / Esc

Printer-friendly Version

Interactive Discussion



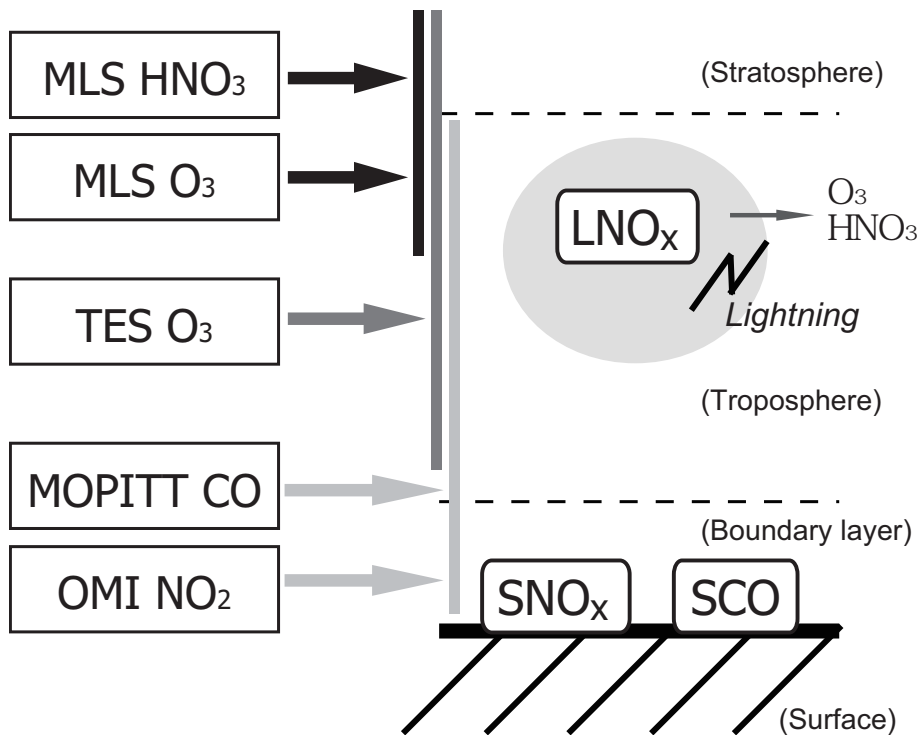


**Fig. 1.** Schematic diagram of the constraints on  $LNO_x$  brought by the different satellite retrieval products. The vertical bars indicate the vertical sensitivity range for the species observed. Through these different sensitivities the assimilation system extracts information about the total  $LNO_x$  source and its profile, the surface emissions, inflows from the stratosphere, and the chemical interactions in the troposphere through the observation of multiple species. Because these sensitivity ranges cover a large part of the troposphere, it is important that the analysis simultaneously optimises the  $LNO_x$  source strength, surface emissions as well as concentrations of the reactive gases involved.

Lightning  $NO_x$   
production  
estimation

K. Miyazaki et al.

Title Page

Abstract

Introduction

Conclusions

References

Tables

Figures

◀

▶

◀

▶

Back

Close

Full Screen / Esc

Printer-friendly Version

Interactive Discussion



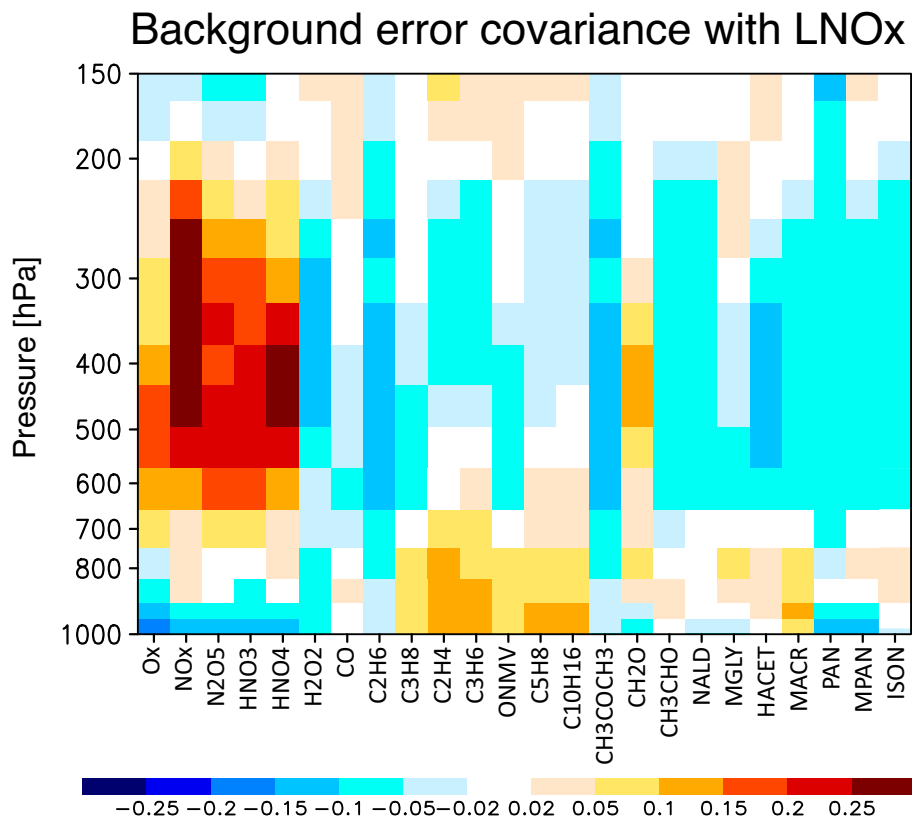


**Fig. 2.** Vertical profiles of correlations between the LNO<sub>x</sub> sources and the concentrations of various chemical species as estimated from the background error covariance matrix based on CHASER ensemble simulations, averaged over central Africa for July 2007. The regional monthly mean of the covariance estimated for each grid point is plotted. The correlation is shown in red or blue where positive or negative, respectively.

**Lightning NO<sub>x</sub> production estimation**

K. Miyazaki et al.

Title Page

Abstract

Introduction

Conclusions

References

Tables

Figures

◀

▶

◀

▶

Back

Close

Full Screen / Esc

Printer-friendly Version

Interactive Discussion



Lightning NO<sub>x</sub>  
production  
estimation

K. Miyazaki et al.

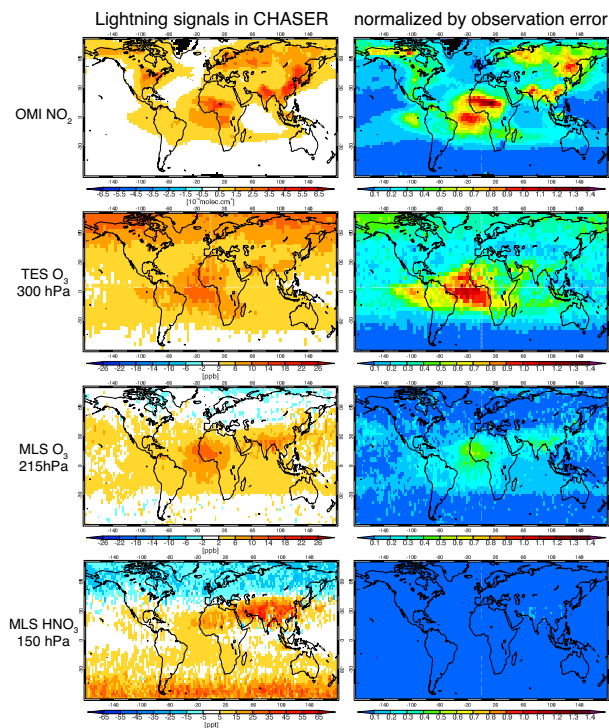


**Fig. 3.** Global maps of (left) the concentration differences between the CHASER simulations with and without lightning sources and (right) the mean ratio of the lightning signals to the measurement errors as estimated along each satellite track by applying the averaging kernels of OMI NO<sub>2</sub> (in 10<sup>14</sup> molec cm<sup>-2</sup>), TES O<sub>3</sub> (ppbv) at 300 hPa, MLS O<sub>3</sub> (ppbv) at 215 hPa, and MLS HNO<sub>3</sub> (pptv) at 150 hPa for June, July, and August in 2007. A super observation approach is employed to the OMI measurements, whereas individual observations are used in the analysis of the others.



Lightning NO<sub>x</sub>  
production  
estimation

K. Miyazaki et al.

Title Page

Abstract

Introduction

Conclusions

References

Tables

Figures



Back

Close

Full Screen / Esc

Printer-friendly Version

Interactive Discussion

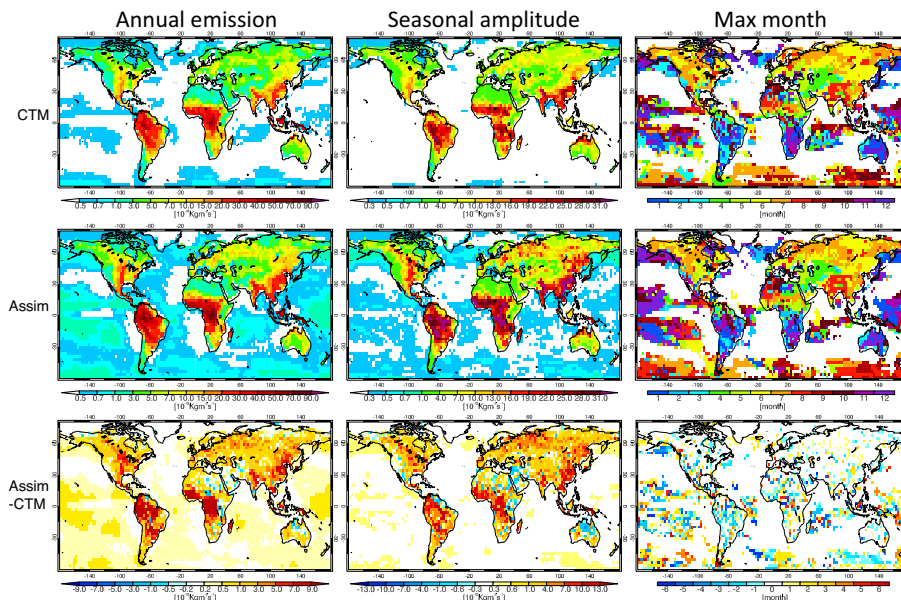


**Fig. 5.** Global distributions of the annual LNO<sub>x</sub> source (left,  $10^{-12} \text{ kg m}^{-2} \text{ s}^{-1}$ ), its seasonal amplitude (centre, in  $10^{-12} \text{ kg m}^{-2} \text{ s}^{-1}$ ), and the timing of peak sources (right, in months) for 2007. Shown are the a priori sources estimated from the CTM parameterisation (upper), the a posteriori sources from the data assimilation (middle), and the analysis increment (lower). The analysis increment equals the a posteriori sources minus the a priori sources. The peak timing is estimated for regions with the analysed annual sources greater than  $0.7 \times 10^{-13} \text{ kg m}^{-2} \text{ s}^{-1}$ .

Lightning NO<sub>x</sub>  
production  
estimation

K. Miyazaki et al.

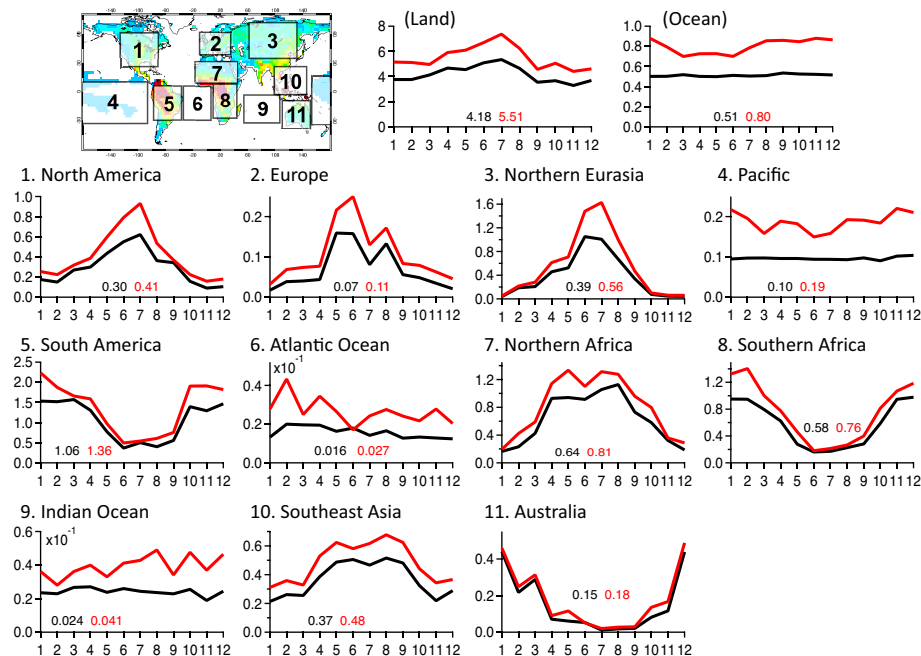


**Fig. 6.** Seasonal variations of the regional LNO<sub>x</sub> sources (in TgN) for (1) North America (120–65° W, 20–60° N), (2) Europe (10° W–30° E, 35–60° N), (3) northern Eurasia (60–130° E, 30–68° N), (4) the Pacific (154–180° E, 35° S–20° N and 180° E–88° W, 35° S–12° N), (5) South America (77–39° W, 35° S–10° N), (6) the Atlantic ocean (35° W–8° E, 30° S–3° N), (7) northern Africa (15° W–48° E, 3–25° N), (8) southern Africa (10–48° E, 30° S–3° N), (9) the Indian ocean (52–108° E, 40–9° S), (10) Southeast Asia (95–146° E, 9° S–26° N), and (11) Australia (112–154° E, 40–12° S). Results for all land areas and for all the oceans are also plotted.

Title Page

Abstract

Introduction

Conclusions

References

Tables

Figures

◀

▶

◀

▶

Back

Close

Full Screen / Esc

Printer-friendly Version

Interactive Discussion

Lightning NO<sub>x</sub>  
production  
estimation

K. Miyazaki et al.

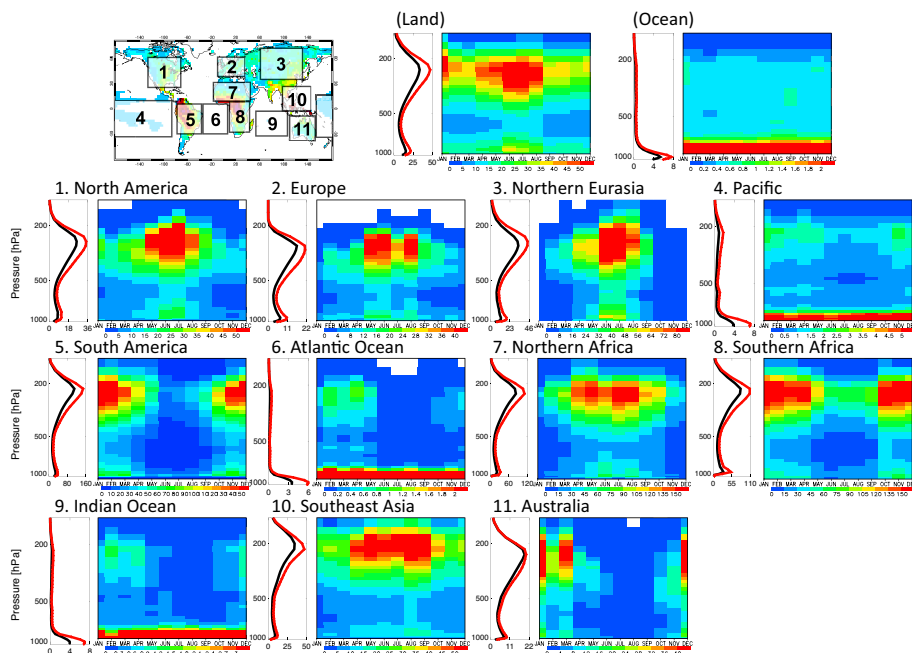


**Fig. 7.** Similar to Fig. 6, but shows for the vertical profile of the annual mean a priori (black) and a posteriori (red) LNO<sub>x</sub> sources (left panels) and the seasonal variation of the monthly mean vertical profile of the a posteriori LNO<sub>x</sub> source (right panels) in pptv day<sup>-1</sup>.

[Title Page](#)
[Abstract](#)
[Introduction](#)
[Conclusions](#)
[References](#)
[Tables](#)
[Figures](#)
[◀](#)
[▶](#)
[◀](#)
[▶](#)
[Back](#)
[Close](#)
[Full Screen / Esc](#)
[Printer-friendly Version](#)
[Interactive Discussion](#)


Lightning  $\text{NO}_x$   
production  
estimation

K. Miyazaki et al.

Title Page

Abstract

Introduction

Conclusions

References

Tables

Figures

◀

▶

◀

▶

Back

Close

Full Screen / Esc

Printer-friendly Version

Interactive Discussion

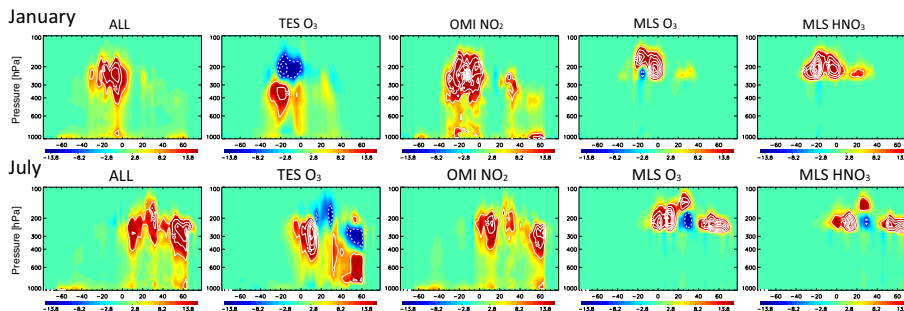


**Fig. 8.** Latitude-pressure cross-sections of the monthly mean analysis increment (the assimilation minus the CTM simulation) for the  $\text{LNO}_x$  source (in  $\text{pptv day}^{-1}$ ) obtained from assimilation of (left) all the data, (2nd from left) TES  $\text{O}_3$  data, (centre) OMI  $\text{NO}_2$  data, (2nd from right) MLS  $\text{O}_3$  data, and (right) MLS  $\text{HNO}_3$  data in (top) January 2007 and (bottom) July 2007. The interval of the contour lines is  $10 \text{ pptv day}^{-1}$ .

Lightning NO<sub>x</sub>  
production  
estimation

K. Miyazaki et al.

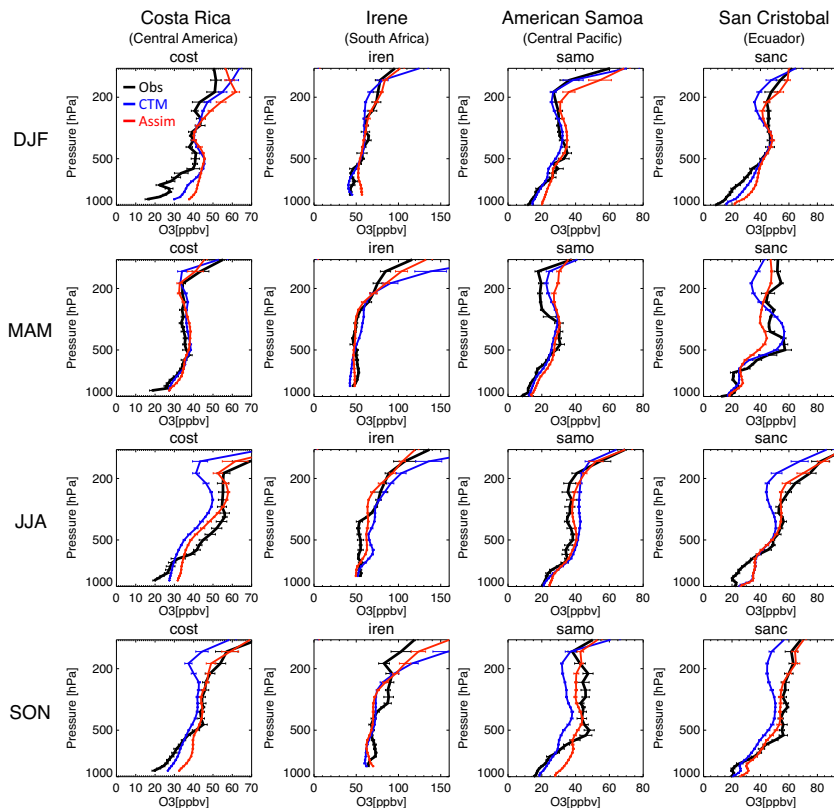


**Fig. 9.** Vertical O<sub>3</sub> profiles (in ppbv) obtained from ozonesondes (black), the CTM simulation (blue), and the data assimilation (red) for Costa Rica (left), Irene in South Africa (2nd from left), American Samoa (2nd from right), and San Cristobal in Ecuador (right) during December–February (DJF, top), March–May (MAM, 2nd from top), June–August (JJA, 2nd from bottom), and September–November (SON, bottom) in 2007. The error bars represent the standard deviation of all the data within one bin.

Title Page

Abstract

Introduction

Conclusions

References

Tables

Figures

◀

▶

◀

▶

Back

Close

Full Screen / Esc

Printer-friendly Version

Interactive Discussion



Lightning NO<sub>x</sub>  
production  
estimation

K. Miyazaki et al.

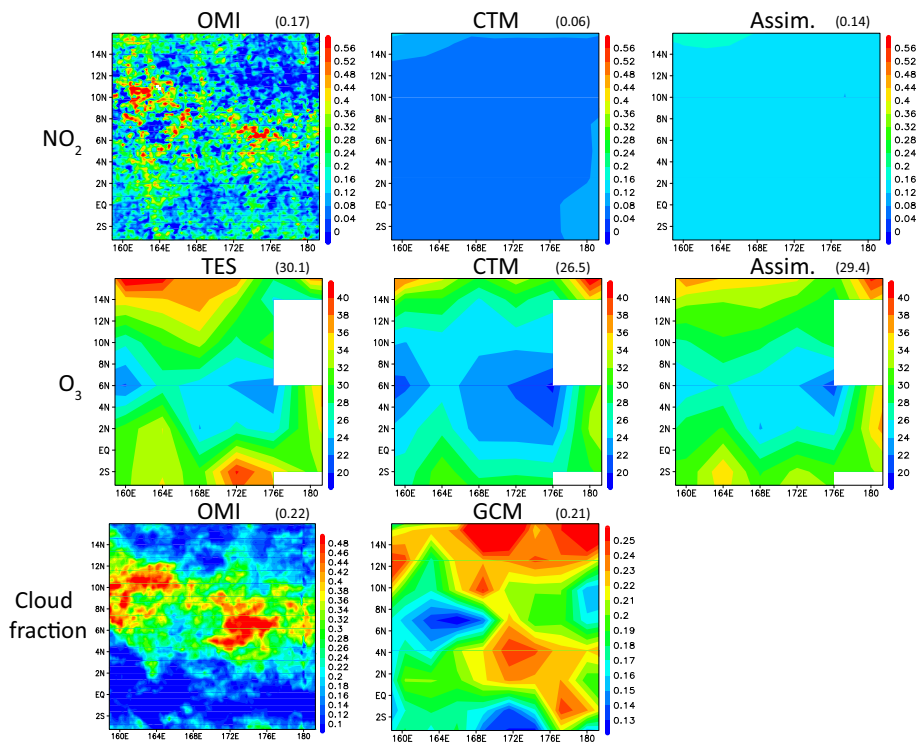


**Fig. 10.** Spatial distributions of tropospheric NO<sub>2</sub> column concentration (upper, 10<sup>15</sup> molec cm<sup>-2</sup>), O<sub>3</sub> concentration at 300 hPa (middle, in ppbv), and cloud fraction (lower) over the western Pacific. Each is averaged over 14–21 August 2007. For the NO<sub>2</sub> and O<sub>3</sub> concentrations, the results obtained from the OMI and TES satellite retrievals (left), the CTM simulation (centre), and the data assimilation (right) are shown. For the cloud fraction, the results obtained from the OMI retrievals (left) and the GCM simulation (centre) are shown. The numbers in brackets represent the regional mean value for each plot.

Lightning  $\text{NO}_x$   
production  
estimation

K. Miyazaki et al.

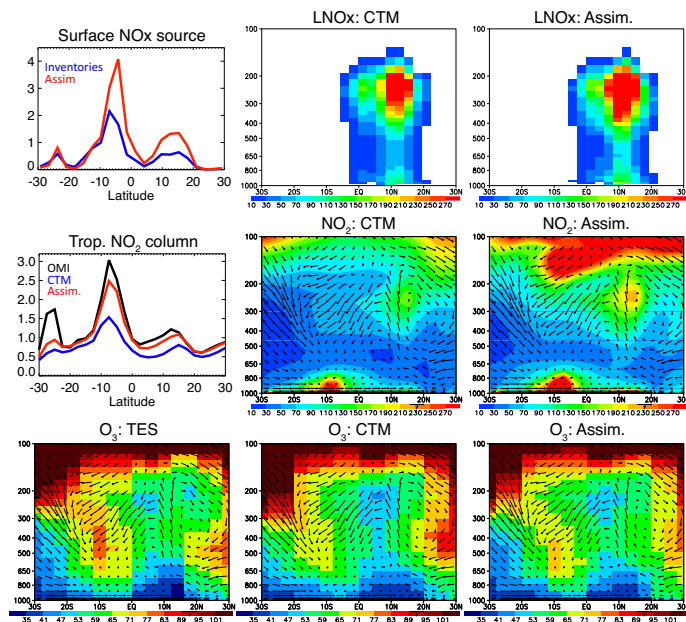


**Fig. 11.** Latitude-pressure cross-section of the longitudinal-mean ( $6^\circ \text{W}$ – $30^\circ \text{E}$ ) of the  $\text{LNO}_x$  source (upper, in  $\text{ppt day}^{-1}$ ),  $\text{NO}_2$  concentration (middle, in pptv), and  $\text{O}_3$  concentration (lower, ppbv) over Africa. The results obtained from the CTM simulation (centre) and the data assimilation (right) are presented. The lower left panel shows the result obtained from the TES measurement for  $\text{O}_3$  concentration. Also shown are the latitudinal distributions of (upper left panel) the longitudinal-mean surface emissions of  $\text{NO}_x$  (in  $10^{-11} \text{ kg m}^{-2} \text{ s}^{-1}$ ) as obtained from the emission inventories (blue line) and the assimilation (red line) and (centre left) the longitudinal-mean tropospheric  $\text{NO}_2$  columns (in  $10^{15} \text{ molec cm}^{-2}$ ) as obtained from the OMI measurements (black line), the CTM simulation (blue line), and the data assimilation (red line). The vectors represent meridional-vertical winds. Each is averaged over 10–20 July 2007.

Lightning  $\text{NO}_x$   
production  
estimation

K. Miyazaki et al.

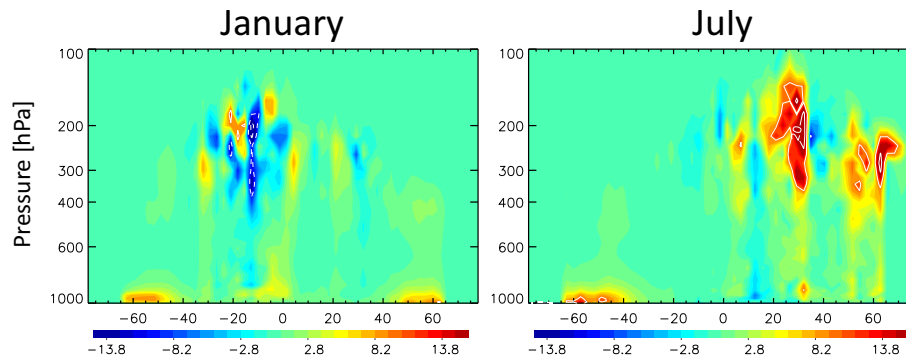


**Fig. 12.** Latitude-pressure cross-section of the  $\text{LNO}_x$  source differences between the data assimilations with and without the cloud-covered OMI  $\text{NO}_2$  observations (in  $\text{pptv day}^{-1}$ ) for January and July in 2007. The increases and decreases in the source due to assimilation of the cloud-covered observations correspond to positive and negative values represented by red and blue, respectively.

[Title Page](#)[Abstract](#)[Introduction](#)[Conclusions](#)[References](#)[Tables](#)[Figures](#)[◀](#)[▶](#)[◀](#)[▶](#)[Back](#)[Close](#)[Full Screen / Esc](#)[Printer-friendly Version](#)[Interactive Discussion](#)